# UNIVERSIDAD DE INVESTIGACIÓN DE TECNOLOGÍA EXPERIMENTAL YACHAY

**Escuela de Ciencias Químicas e Ingeniería**

**TÍTULO: Small Organic Molecules and Conducting Polymers as Hole Extracting Layers in Organic Photovoltaic Devices**

Trabajo de integración curricular presentado como requisito para la obtención del título de Químico

**Autor:**

Karla Sofía Pavón Ipiales

**Tutor:**

Dr. Alex Uriel Palma Cando

**Cotutor:**

Dr. Bernardo Frontana Uribe

Urcuquí, Abril de 2021

## SECRETARÍA GENERAL
### (Vicerrectorado Académico/Cancillería)
### ESCUELA DE CIENCIAS QUÍMICAS E INGENIERÍA
### CARRERA DE QUÍMICA
### ACTA DE DEFENSA No. UITEY-CHE-2021-00003-AD

A los 11 días del mes de mayo de 2021, a las 11:00 horas, de manera virtual mediante videoconferencia, y ante el Tribunal Calificador, integrado por los docentes:

| | |
|---|---|
| Presidente Tribunal de Defensa | Dra. LOPEZ GONZALEZ, FLORALBA AGGENY , Ph.D. |
| Miembro No Tutor | Dra. RODRIGUEZ CABRERA, HORTENSIA MARIA , Ph.D. |
| Tutor | Dr. PALMA CANDO, ALEX URIEL , Ph.D. |

El(la) señor(ita) estudiante **PAVON IPIALES, KARLA SOFIA**, con cédula de identidad No. **1004281125**, de la **ESCUELA DE CIENCIAS QUÍMICAS E INGENIERÍA**, de la Carrera de **QUÍMICA**, aprobada por el Consejo de Educación Superior (CES), mediante Resolución **RPC-SO-39-No.456-2014**, realiza a través de videoconferencia, la sustentación de su trabajo de titulación denominado: **SMALL ORGANIC MOLECULES AND CONDUCTING POLYMERS AS HOLE EXTRACTING LAYERS IN ORGANIC PHOTOVOLTAIC DEVICES**, previa a la obtención del título de **QUÍMICO/A**.

El citado trabajo de titulación, fue debidamente aprobado por el(los) docente(s):

| | |
|---|---|
| Tutor | Dr. PALMA CANDO, ALEX URIEL , Ph.D. |

Y recibió las observaciones de los otros miembros del Tribunal Calificador, las mismas que han sido incorporadas por el(la) estudiante.

Previamente cumplidos los requisitos legales y reglamentarios, el trabajo de titulación fue sustentado por el(la) estudiante y examinado por los miembros del Tribunal Calificador. Escuchada la sustentación del trabajo de titulación a través de videoconferencia, que integró la exposición de el(la) estudiante sobre el contenido de la misma y las preguntas formuladas por los miembros del Tribunal, se califica la sustentación del trabajo de titulación con las siguientes calificaciones:

| Tipo | Docente | Calificación |
|---|---|---|
| Tutor | Dr. PALMA CANDO, ALEX URIEL , Ph.D. | 9,9 |
| Presidente Tribunal De Defensa | Dra. LOPEZ GONZALEZ, FLORALBA AGGENY , Ph.D. | 10,0 |
| Miembro Tribunal De Defensa | Dra. RODRIGUEZ CABRERA, HORTENSIA MARIA , Ph.D. | 10,0 |

Lo que da un promedio de: **10 (Diez punto Cero)**, sobre 10 (diez), equivalente a: **APROBADO**

Para constancia de lo actuado, firman los miembros del Tribunal Calificador, el/la estudiante y el/la secretario ad-hoc.

Certifico que *en cumplimiento del Decreto Ejecutivo 1017 de 16 de marzo de 2020, la defensa de trabajo de titulación (o examen de grado modalidad teórico práctica) se realizó vía virtual, por lo que las firmas de los miembros del Tribunal de Defensa de Grado, constan en forma digital.*

**PAVON IPIALES, KARLA SOFIA**
**Estudiante**

FLORALBA AGGENY LOPEZ GONZALEZ
Digitally signed by FLORALBA AGGENY LOPEZ GONZALEZ
Date: 2021.05.11 12:17:51 -05'00'

**Dra. LOPEZ GONZALEZ, FLORALBA AGGENY , Ph.D.**
**Presidente Tribunal de Defensa**

Dr. PALMA CANDO, ALEX URIEL , Ph.D.
**Tutor**

Firmado electrónicamente por:
**ALEX URIEL
PALMA CANDO**

Dra. RODRIGUEZ CABRERA, HORTENSIA MARIA , Ph.D.
**Miembro No Tutor**

HORTENSIA MARIA RODRIGUEZ CABRERA

Firmado digitalmente por HORTENSIA MARIA RODRIGUEZ CABRERA
Fecha: 2021.05.11 15:19:02 -05'00'

CIFUENTES TAFUR, EVELYN CAROLINA
**Secretario Ad-hoc**

EVELYN CAROLINA CIFUENTES TAFUR

Digitally signed by EVELYN CAROLINA CIFUENTES TAFUR
Date: 2021.05.11 12:20:30 -05'00'

# AUTORIA

Yo, Karla Sofía Pavón Ipiales, con cédula de identidad 1004281125, declaro que las ideas, juicios, valoraciones, interpretaciones, consultas bibliográficas, definiciones y conceptualizaciones expuestas en el presente trabajo, así como, los procedimientos y herramientas utilizadas en la investigación, son de absoluta responsabilidad del autor del trabajo de integración curricular. Así mismo, me acojo a los reglamentos internos de la Universidad de Investigación de Tecnología Experimental Yachay.

Urcuquí, abril 2021

Karla Sofía Pavón Ipiales
CI: 1004281125

# AUTORIZACIÓN DE PUBLICACIÓN

Yo, Karla Sofía Pavón Ipiales, con cédula de identidad 1004281125, cedo a la Universidad de Investigación de Tecnología Experimental Yachay, los derechos de publicación de la presente obra, sin que deba haber un reconocimiento económico por este concepto. Declaro además que el texto del presente trabajo de titulación no podrá ser cedido a ninguna empresa editorial para su publicación u otros fines, sin contar previamente con la autorización escrita de la Universidad.

Así mismo, autorizo a la Universidad que realice la digitalización y publicación de este trabajo de integración curricular en el repositorio virtual, de conformidad a lo dispuesto en el Art. 144 de la Ley Orgánica de Educación Superior.

Urcuquí, abril 2021

Karla Sofía Pavón Ipiales
CI: 1004281125

*A mis padres.*

# Acknowledgments

I would like to thank to:

My parents for their love, understanding and support.

My fellow students at Yachay Tech.

My tutor Dr. Alex Palma Cando who guided me in the development of this work.

Professors of Yachay Tech for their labor.

Proyects CHEM19-17 YT and PAPIIT IN208919 DGAPA UNAM

My co-advisor Dr. Bernardo Frontana Uribe and the members of the jury, Floralba López and Hortensia Rodriguez for their comments that boosted the quality of this thesis.

Karla Pavón

## Resumen

La demanda mundial de energía está aumentando, por lo que son fundamentales las fuentes de energía renovables emergentes, como las celdas solares, que mitigan el efecto negativo del consumo de combustibles fósiles. Las celdas solares orgánicas (OSCs, por sus siglas en inglés), cuya capa fotoactiva está compuesta por polímeros o moléculas orgánicas, tienen algunas ventajas como la rapidez y el bajo costo de producción, el procesamiento en solución, el bajo tiempo de recuperación de la energía, la ligereza y un menor impacto medioambiental adverso. La mejora de la eficiencia y la estabilidad de las OSCs son fundamentales. En este sentido, se ha explorado el uso de la capa de transporte de agujeros (HTL, por sus siglas en inglés) basada en materiales orgánicos por su alto impacto en la eficiencia de conversión de energía y la estabilidad de las OSCs y por ser adecuada para la producción masiva (e.g., tecnología rollo a rollo). Este trabajo presenta una revisión del estado del arte de la investigación sobre polímeros conductores, sus compósitos y pequeñas moléculas orgánicas utilizadas como HTLs en las OSCs, destacando las mejoras en los parámetros fotovoltaicos y la estabilidad de los OSCs. Esta revisión bibliográfica considera las publicaciones científicas más relevantes realizadas desde 2016 hasta 2020.


**Palabras clave:** Capa de transportadora de agujeros, polímeros conductores, polielectrolitos conjugados, pequeñas moléculas orgánicas, celdas solares orgánicas, eficiencia de fotoconversión.

# Abstract

Global energy demand is increasing; thus, emerging renewable energy sources, like solar cells, are fundamental to mitigate fossil fuels consumption negative effect. Organic solar cells (OSCs), which polymers or organic molecules compose photoactive layer, have some advantages such as fast and low-cost production, solution process, low energy payback time, light weight and less adverse environmental impact. Improvements in OSCs efficiency and stability are fundamental. In this way, the use of hole transport layers (HTLs) based on organic materials is explored because its high impact on OSCs' power conversion efficiency and stability and suitable for roll-to-roll production. This work presents a state-of-the-art review of the research about conducting polymers and small organic molecules used as HTL in OSCs, highlighting the improvements in device photovoltaic parameters and OSCs' stability. This review considers high-impact scientific publications from 2016 to 2020. OSCs' stability

**Keywords:** Hole transport layer, conducting polymers, conjugated polyelectrolyte, small organic molecules, organic solar cells, photoconversion efficiency.

**INDEX**

# ABBREVIATIONS AND ACRONYMS

| | |
|---|---|
| **AIL** | Anode interfacial layer |
| **BF-DPB** | N,N'-((diphenyl-N,N'-bis)9,9,-dimethyl-fluoren-2-yl)-benzidine |
| **bf-MWCNTs** | Boronic acid functionalized multi-walled carbon nanotubes |
| **BHJ** | Bulk heterojunction |
| **BPQDs** | Black phosphorous quantum dots |
| **CBP** | 4,4′-N,N′-dicarbazole-biphenyl |
| **CIGS** | Copper indium gallium diselenide |
| **CNT** | Carbon nanotubes |
| **CPE** | Conjugated polyelectrolytes |
| **DA** | Dopamine |
| **DIPO-Ph$_4$** | 2,2',6,6'-tetraphenyl-dipyranylidene |
| **DMSO** | Dimethyl sulfoxide |
| **EGME** | 2-methoxyethanol |
| **EQE** | External quantum efficiency |
| **ETL** | Electron transport layer |
| **F4-TCNQ** | 2,3,5,6-tetrafluoro-7,7,8,8-tetracyanoquinodimethane |
| **FBT-TH4** | Poly 5,6-difluorobenzothiadiazole |
| **FF** | Fill factor |
| **g-C$_3$N$_4$** | Graphitic carbon nitrile |
| **GO** | Graphene oxide |
| **GSL** | Grafted sulfonated-acetone-formaldehyde lignin |
| **HOMO** | Highest occupied molecular orbital |
| **HPCzI** | 1,3,4,5,6,7-hexaphenyl-2-{3'-(9-ethylcarbazolyl)}-isoindole |
| **HTL** | Hole transport layer |
| **ICBA** | 1′,1″,4′,4″-Tetrahydro-di[1,4]methanonaphthaleno[1,2:2′,3′,56,60:2″,3″][5,6]fullerene-C60 |
| **IDIC** | 2,2'-[(4,4,9,9-tetrahexyl-4,9-dihydro-s-indaceno[1,2-b:5,6-b']dithiophene-2,7-diyl)bis[methylidyne(3-oxo-1H-indene-2,1(3H)-diylidene)]]bis-propanedinitrile |
| **IPA** | Isopropanol |
| **IT-4F** | 3,9-bis(2-methylene-((3-(1,1-dicyanomethylene)-6,7-difluoro)-indanone))-5,5,11,11-tetrakis(4-hexylphenyl)-dithieno[2,3-d:2',3'-d']-s-indaceno[1,2-b:5,6-b']dithiophene |
| **ITIC** | 3,9-bis(2-methylene(3-(1,1-dicyanomethylene)-indanone))-5,5,11,11-tetrakis(4-hexylphenyl)dithieno-[2,3-d:2',3'-d']-s-indaceno[1,2-b:5,6-b']dithiophene |
| **ITIC-Th** | 3,9-bis(2-methylene-(3-(1,1-dicyanomethylene)-indanone))-5,5,11,11-tetrakis(5-hexylthienyl)-dithieno[2,3-d:2',3'-d']-s-indaceno[1,2-b:5,6-b']dithiophene |
| **ITO** | Indium tin oxide |
| **J$_{sc}$** | Short circuit current |

| | |
|---|---|
| **LIL** | Laser interference lithography |
| **LSPR** | Localized surface plasmon resonance |
| **LUMO** | Lowest unoccupied molecular orbital |
| **MeOPhN-DBC** | Dibenzo[g,p]chrysene derivative, 3,6,11,14-tetramethoxyphenylamine- dibenzo[g,p]chrysene |
| **MMP** | Maximum power output |
| **MO** | Metal oxides |
| **ND** | Nanodot |
| **NFD** | Nickel formate dihydrate |
| **nGQDs** | Nitrogen doped graphene quantum dots |
| **NPB** | N, N′-bis(1-naphthalenyl)N,N′-bis-phenyl-(1, 1′-biphenyl)-4, 4′-diamine |
| **NPs** | Nanoparticles |
| **NRs** | Nanorods |
| **NWs** | Nanowires |
| **O-IDTBR** | (5Z,5'Z)-5,5'-{[7,7'-(4,4,9,9-tetraoctyl-4,9-dihydro-s-indaceno[1,2-b:5,6-b']dithiophene-2,7-diyl)bis(benzo[c][1,2,5]thiadiazole-7,4-diyl)]bis(methanylylidene)}bis(3-ethyl-2-thioxothiazolidin-4-one) |
| **OLEDs** | Organic light-emiting diodes |
| **OSC** | Organic solar cell |
| **P3HT** | Poly(3-hexylthiophene) |
| **P3HT$_{50}$-b-PSS$_{23}$** | Poly(3-hexylthiophene)-*b*-poly(p-styrenesulfonate) |
| **P3HTN** | Poly[3-(6'-N,N,N-trimethyl ammonium)-hexylthiophene] bromide |
| **P3HT-Si** | Triethoxysilane terminated poly(3-hexylthiophene) |
| **PANI** | Polyaniline |
| **PBDB-T** | Poly[(2,6-(4,8-bis(5-(2-ethylhexyl)thiophen-2-yl)benzo[1,2-b:4,5-b']dithiophene)-co-(1,3-di(5-thiophene-2-yl)-5,7-bis(2-ethylhexyl)benzo[1,2-c:4,5-c']dithiophene-4,8-dione)] |
| **PBDT-DTNT** | Poly[benzodithiophene-bis(decyltetradecyl-thien)naphthothiadiazole] |
| **PBDT-TS1** | Poly[4,8-bis(5-(octylthio)thiophen-2-yl)benzo[1,2-b;4,5-b']dithiophene-2,6-diyl–alt–(4-(2-ethylhexyl)-3-fluorothieno[3,4-b]thiophene-)-2-carboxylate-2-6-diyl] |
| **PC** | Phthalocyanine |
| **PC$_{71}$BM** | (6,6)-phenyl-C71-butyric acid methyl ester |
| **PCBM** | Phenyl-C61-butyric acid methyl ester |
| **PCDTBT** | Poly[N-9'-heptadecanyl-2,7-carbazole-alt-5,5(4',7'-di-2-thienyl-2',1',3'-benzothiadiazole)] |
| **PCE** | Power conversion efficiency |
| **PCPDT** | Poly 3,4-dithia-7H-cyclopenta[a]pentalene |
| **PCP-Na** | Poly[2,6-(4,4-bis-(propane-1-sulfonate sodium)-4H-cyclopenta[2,1-b ;3,4-b' ]dithiophene)-alt-(4,4′-biphenyl)] |
| **PDMS** | Poly(dimethylsiloxane) |
| **PDMT** | Poly(3,4-dimethoxythiophene) |
| **PEDOT** | Poly(3,4-ethylenedioxythiophene) |

| | |
|---|---|
| **PEDOT-S** | Poly(4-(2,3-dihydrothieno[3,4-b][1,4]dioxin-2-yl-methoxy)-1-butanesulfonic acid) |
| **PEG** | Polyethylene glycol |
| **PffBT4T-2OD** | Poly[(5,6-difluoro-2,1,3-benzothiadiazol-4,7-diyl)-alt-(3,3'''-di(2-octyldodecyl)-2,2';5',2'';5'',2'''-quaterthiophen-5,5'''-diyl)] |
| **PFN** | Poly[(9,9bis(3'-(N,N-dimethylamino)propyl)-2,7-fluorene)-alt-2,7-(9,9dioctylfluorene)] |
| **PFSe** | Poly[9,9-bis(4′-sulfonatobutyl)fluorene-alt-selenophene] |
| **PFT-D** | Poly[9,9-bis(4′-sulfonatobutyl)fluorene-*alt*-thiophene] |
| **PFtT-D** | Poly[9,9-bis(4'-sulfonatobutyl)fluorene-alt-thieno[3,2-b]thiophene] |
| **PhNa-1T** | Poly[1,4-bis(4-sulfonatobutoxy)benzene-thiophene] |
| **$P_{in}$** | Input power |
| **PL** | Photoluminescence |
| **PM6** | Poly[(2,6-(4,8-bis(5-(2-ethylhexyl)-4-fluorothiophen-2-yl)benzo[1,2-b:4,5-b']dithiophene))-co-(1,3-di(5-thiophene-2-yl)-5,7-bis(2-ethylhexyl)-benzo[1,2-c:4,5-c']dithiophene-4,8-dione))] |
| **PM6** | Poly[(2,6-(4,8-bis(5-(2-ethylhexyl)-4-fluorothiophen-2-yl)benzo[1,2-b:4,5-b']dithiophene))-co-(1,3-di(5-thiophene-2-yl)-5,7-bis(2-ethylhexyl)-benzo[1,2-c:4,5-c']dithiophene-4,8-dione))] |
| **PMA** | Phosphomolybdic acid |
| **PMMA** | Poly(methylmethacrylate) |
| **PNDIT-F3N** | Poly[[2,7-bis(2-ethylhexyl)-1,2,3,6,7,8-hexahydro-1,3,6,8-tetraoxobenzo[lmn] [3,8]phenanthroline-4,9-diyl]-2,5-thiophenediyl[9,9-bis[3'((N,N-dimethyl)-N-ethylammonium)]propyl]-9H-fluorene-2,7-diyl]-2,5-thiophenediyl] |
| **$P_{out}$** | Output power |
| **PSC** | Polymer solar cell |
| **PSFP-DTBTP** | Poly[(9,9-bis(4-sulfonatobutyl sodium) fluorene-alt-phenylene)-ran-(4,7-di-2-thienyl-2,1,3-benzothiadiazole-alt-phenylene)] |
| **PSS** | Poly(styrenesulfonate) |
| **PTB7** | Poly [[4,8-bis[(2-ethylhexyl)oxy]benzo[1,2-b:4,5-b']dithiophene-2,6-diyl][3-fluoro-2-[(2-ethylhexyl)carbonyl]thieno[3,4-b]thiophenediyl]] |
| **PTB7-Th** | Poly[4,8-bis(5-(2-ethylhexyl)thiophen-2-yl)benzo[1,2-b;4,5-b']dithiophene-2,6-diyl-alt-(4-(2-ethylhexyl)-3-fluorothieno[3,4-b]thiophene-)-2-carboxylate-2-6-diyl)] |
| **p-TPCF** | Polytriphenylcarbazole fluoranthene |
| **PTPCz** | Poly(carbazolyl triphenylethylene) derivative |
| **PV** | Photovoltaic |
| **QDs** | Quantum dots |
| **rrP3HT** | Regioregular poly(3-hexylthiophene-2,5-diyl) |
| **$R_s$** | Series resistance |
| **$R_{sh}$** | Shunt resistance |
| **TEMPO** | 2,2,6,6-tetramethylpiperidine-1-oxoammonium |
| **TFB** | Poly[(9,9-dioctylfluorenyl-2,7-diyl)-alt-(4,4'-(N-(4-butylphenyl)))] |
| **TTA** | Tetrathiafulvalene |
| **TTF-py** | Tetrathiafulvalene pyridine derivative |

| | |
|---|---|
| **uSWNT** | Unzipped single-walled carbon nanotubes |
| **UVO** | UV-ozone |
| **$V_{oc}$** | Open circuit voltage |
| **VoPC** | Vanadylphthalocyanine |
| **WF** | Work function |
| **Y6** | (2,2'-((2Z,2Z)-((12,13-bis(2-ethylhexyl)-3,9-diundecyl-12,13-dihydro-[1,2,5]thiadiazolo[3,4-e]thieno[2,"3":4',50]thieno[2',3':4,5]pyrrolo[3,2-g]thieno[2',3':4,5]thieno[3,2-b]indole-2,10-diyl)bis(methanylylidene))bis(5,6-difluoro-3-oxo-2,3-dihydro-1H-indene-2,1-diylidene))dimalononitrile) |
| **$\mu_h$** | Hole mobility |
| **$\mu_e$** | Electron mobility |

# LIST OF FIGURES

# 1 INTRODUCTION

## 1.1 General Introduction

Global energy consumption keeps growing; the energy demand increased slowly in 2019 compared to 2018, i.e., 120 million tons of oil equivalent (Mtoe) [1]. The expansion of energy consumption, the energy sources used, and the consequences of their utilization represent some of the most important problems that face humanity [2]. World energy consumption is covered mainly by fossil fuels' energy sources (coal, oil, natural gas), with 84.3% of total consumption. Nuclear energy represents 4.3% of total consumption, while renewable energy sources such as wind, solar, hydropower, and biomass only represent about 11.4% [3] (see Figure 1). The world oil demand grew by 0.8%, while natural gas had grown by 1.8% in 2019. Global coal demand declined 1.7%; however, it is still one of the largest sources. Renewables (440 terawatt hour (TWh)) and nuclear energy (95 TWh) produced more electricity than coal by 2019. The role of renewable energy sources has to gain importance, as a consequence of the expansion of wind energy (150 TWh), photovoltaics (140 TWh), and hydropower (100 TWh). Renewable energy use increased by 3.7% in 2019 [1]. Fossil fuel energy is low cost, but it is based on finite sources; their reserves will be depleted [2]. Its large use and the $CO_2$ emission from fossil fuel power plants have been cause a great impact on climate change and the environment, which threaten the quality of life.

Furthermore, the problems related to nuclear energy sources involve the management of high-level radioactive waste, the possibility of nuclear accidents, and the availability of uranium reserves that are also depletable resources [2]. The share of renewable energy sources increases; carbon emission growth in 2019 slowed down due to primary energy consumption decreased, and renewables and natural gas increased [1]. One cause for the growth in energy requirements is the growth of the world population; the current population is around 7.8 billion people, and it is expected to rise to more than 10 billion people by 2055 [4].
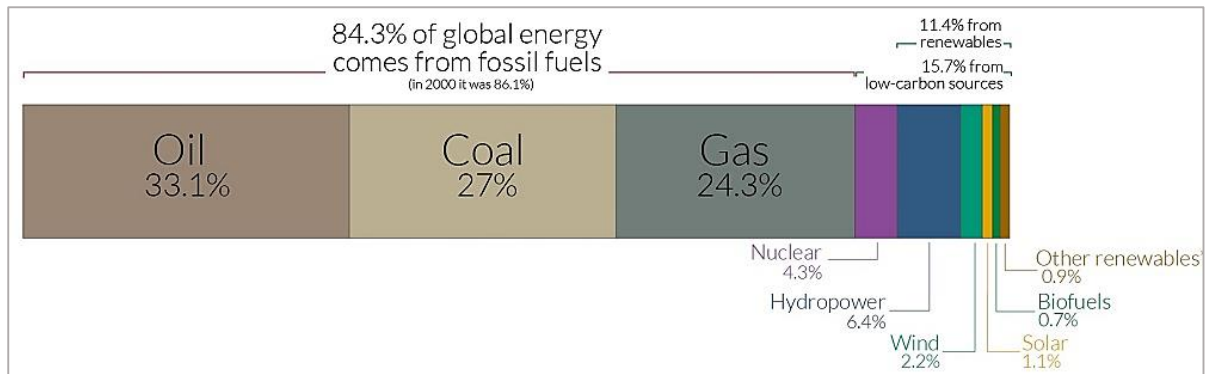
Figure 1. Global primary energy consumption by source. Other renewables include geothermal, biomass, wave, and tidal [5].

Renewable energies mean that the supply of energy is not depleted or naturally replenished on a human timescale. Renewable energies allow the transition to a less carbon-intensive and more sustainable energy system. These renewables have grown in recent years by the policy support and the cost reductions for solar cells and wind power [1]. Solar radiation is related to hydropower because it is only possible by the evaporation of water, wind power that depends on atmospheric movement, and biomass that is only possible through photosynthesis. Photovoltaic devices (PVs) or solar cells (SCs) directly convert solar radiation into electrical energy without pollution. Besides, solar energy is abundantly available. Among different solar cells the silicon cells dominate the market; they show a good performance and high stability. Thin-film solar cells are based on scarce or toxic elements such as cadmiun telluride (CdTe), copper indium gallium diselenide (CIGS), and GaAs cells. Other solar cells include amorphous silicon and the emerging PVs cells that include dye-sensitized cells, multijunction cells, perovskite cells, quantum dot solar cells, and organic solar cells (OSCs) [6]. Some companies have developed OSCs commercially, such as Heliatek, infinityPV, and OPVIUS GmbH, which manufacture flexible OSC modules [7]. Organic PVs have been used in small-scale applications, building integrated photovoltaics, i.e., incorporated on the roofs and walls of storage buildings [8], and a solar park based on polymer solar cells has also been installed [9]. OSCs have some advantages: low-cost fabrication, solution processes, lightweight, flexibility, a great opportunity for large-scale roll–to-roll production, and a low environmental disposable impact. OSCs are non-toxic and use non-scarce materials. Furthermore, OSCs showed shortened energy payback time; this is the time needed to recover the device fabrication energy [2]. OSCs record efficiency are over 18.2% [10, 11] and over 18.6% in tandem organic solar cells [12].

The core of the OSCs is a blend of electron-donor materials (e.g., polymers easily oxidized) and fullerene-based or non-fullerene-based as electron-acceptor materials [13], which are easily reduced. This central layer is called the photoactive layer and absorbs solar illumination. A typical OSC has a bulk heterojunction (BHJ) structure that is a mixed-blend of donor and acceptor materials, which constitute the photoactive layer [14]. OSCs configuration includes several layers (see Figure 2), (i) a transparent substrate is coated with a transparent conductor as anode like indium tin oxide (ITO), (ii) between the anode and photoactive layer is a hole transport layer (HTL) commonly poly(3,4ethylenedioxythiophene):poly(styrene sulfonate) (PEDOT:PSS), and (iii) over the active layer is an electron transport layer (ETL) followed by a cathode. Depending on the charge flow direction, OSCs can be conventional or inverted devices (Figure 2 (a), (b)). When solar cell is irradiated by solar radiation, photoactive layer absorbs photons to generate excitons (bound electron-hole pair), which dissociate into free charge carriers in the donor-acceptor interface producing separated holes and electrons. These free charges are then extracted and transported to the corresponding electrodes [15, 16].
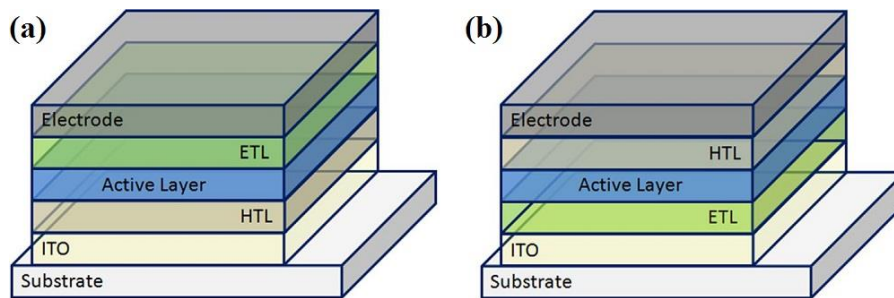


Figure 2. Different device architectures of BHJ solar cell. (a) Standard device configuration and (b) inverted device architecture [15].

The power of a solar cell is measured through a characteristic current density-voltage curve (J-V curve). A J-V curve corresponds to a diode principle and describes the solar energy conversion ability and efficiency of a solar cell. Parameters used to describe the device performance are (i) the open-circuit voltage ($V_{OC}$) that is the maximum voltage that a solar cell can supply when an infinite load is applied, and (ii) the short circuit current ($J_{sc}$) that is the maximum current of the solar cell under the condition of a zero resistance load [17]. The maximum power output (MMP) is the maximum value resultant of the product of voltage and current along the J-V curve. The fill factor (FF) is given by the ratio of the maximum power

produced by the solar cell to the product of $V_{OC}$ and Jsc. FF term is used as a quality parameter for solar cells [18].

$$FF = \frac{V_{MPP} \times J_{MPP}}{V_{OC} \times J_{SC}}$$

Power conversion efficiency (PCE) describes the efficiency of the solar cell, and it is determined by the ratio of the output power ($P_{out}$) (generated electrical energy per unit time) to the input power ($P_{in}$) (incoming electromagnetic radiation per unit time) [18, 19].

$$PCE = \left(\frac{P_{out}}{P_{in}}\right) \times 100 = \frac{FF \times V_{OC} \times J_{SC}}{P_{in}} \times 100$$

Interfacial layers (e.g., ETLs and HTLs) are generally utilized to tailor the work function of electrodes for charge carrier collection maximization, modify the interface to alter the photoactive layer morphology, and minimize charge carrier recombination (improving the charge selectivity) at the interface between the active layer and transport layer [20]. Besides, the interfacial layers help to form an ohmic contact between electrodes and active layers, and tune the energy level alignment between electrodes and active layer to facilitate the charge extraction [21, 22]. HTLs, also called anode interfacial layer (AIL), facilitate hole extraction and transportation while blocking electrons flux. Hole transport materials are deposited between the photoactive layer and the anode improving the device performance. HTLs, used in conventional polymer solar cells (PSCs), were first reported in the late 1990s after a similarly reported experimentation in organic light-emitting diodes (OLEDs) [23, 24]. For hole transport materials; some important characteristics are required, as for example a high conductivity, high transparency since the sunlight is absorbed by the photoactive layer through the HTL on anode, solution processability and favorable stability, high work function, since the energy level of materials should be appropriate for charge collection and predominant good hole mobility [25].

## 1.2 Problem Statement

Nowadays, the interest in a greener energy supply increases to combat climate change and mitigate the negative consequences of the consumption of fossil fuels. Furthermore, the need for renewable and sustainable energy supplies appears to be essential to not endangering future generations. Although renewable energy sources as wind, hydropower, solar, and biomass still represent a small fraction of energy sources [3]. The research community is focused in achieving high efficiency and low cost of production of emerging clean energy sources. Solar cells produce electrical energy directly from solar radiation. OSCs have some advantages such as fast production, low-cost manufacturing processes and a reduced energy payback time [26]. The interfacial layers as HTLs allow for improving the device performance and stability of OSCs [23]. In this sense, HTLs based on conducting polymers and small organic molecules offer the opportunity to enhance OSCs' device performance.

An extensive state-of-the-art review is reported in this work, focusing on the conducting polymers and small organic molecules and their composites used as HTLs in OSCs. The contribution of HTLs to the photovoltaic device performance is explored, leading to improvements in device parameters as $V_{oc}$, $J_{sc}$, FF, PCE, and device stability.

## 1.3 General and Specific Objectives

- **General Objective**

To generate a state-of-the-art review in the hole transport layer based on conducting polymers and small organic molecules in organic solar cells.

- **Specific Objectives**

To compile and analyze the most relevant reported research over the last five years about:

Conducting polymers and their composites used as HTL in OSCs.

Conjugated polyelectrolyte materials used as HTL in OSCs.

Small organic molecules used as HTL in OSCs.

## 2    STATE-OF-THE-ART REVIEW

### 2.1    Conducting polymers and their composites

#### 2.1.1    PEDOT and its modifications

Poly(3,4-ethylenedioxythiophene):polystyrene sulfonate (PEDOT:PSS) (see the structure in Figure 11) is the most common conducting polymer [27] used as hole transporting material in organic solar cells (OSCs) due to its easy solution processing, suitable work function (WF) around 5.1 eV, high conductivity, good transparency, good mechanical properties and adapted wettability on the bulk heterojunction (BHJ) layer. For instance, patterning interfacial PEDOT:PSS layer formed by a nanoimprinting technique using poly(dimethylsiloxane) (PDMS) stamp was employed on OSCs based on poly(3-hexylthiophene):phenyl-C61-butyric acid methyl ester (P3HT:PCBM) showing an increased PCE of 1.53% (compared to a PCE of 1.1% for a reference device made of spin-coated PEDOT:PSS directly onto ITO glass substrate) [28]. Also, when PEDOT:PSS was incorporated on an inverted OSC based on P3HT:O-IDTBR with evaporated Ag back electrode showed an enhanced device performance [29]. The incorporation of PEDOT:PSS into P3HTN:PEG-C$_{60}$ based OSCs increased the V$_{oc}$ to 1.3 V, but the FF decreased concerning a device employing bare ITO [30]. The OSC showed a PCE of 0.23% attributed to the large collection barrier.

PEDOT:PSS has strong acidic nature due to the polystyrene sulfonate (PSS) (pH ~ 2), which deteriorates the anode material and the photoactive layer affecting the performance and stability of the device. Besides, this polyelectrolyte has high affinity for environmental water (hygroscopic) making necessary to encapsulate the OSC´s before durability test; humidity is a major problem in these devices. According to that, different modifications to PEDOT:PSS layer have been developed to overcome these issues. Some post-treatments to PEDOT:PSS layer have been tested using solvents [31], surfactants [32], and by exchange of PSS with less acidic dopants as well as the addition of small molecules [33–36]. These modifications aim to reach a uniform morphology, increase the interface contact, and produce a neutral pH hole-transporting polymer to improve the stability and cell performance. The use of a layer composed of PEDOT and grafted sulfonated-acetone-formaldehyde lignin (GSL) instead of PSS resulted in a better photovoltaic performance than conventional PEDOT:PSS [35]. GSL is a less acidic copolymer of lignin. A quite homogeneous surface of the HTL for a cell architecture ITO/PEDOT:GSL/PTB7-Th:PC$_{71}$BM/poly[(9,9bis(3'-(N,N-dimethylamino)propyl)-2,7-fluorene)-alt-2,7-(9,9dioctylfluorene)] (PFN)/Al resulted in a

PCE of 8.47%. PEDOT:PSS treatment with solvents as isopropanol (IPA) also shows a better performance mainly due to more uniform morphology, increased current density, and improved cell light absorption [31].

2-Methoxyethanol (EGME) and dimethyl sulfoxide (DMSO) solvents were added to a PEDOT:PSS solution. The conductivity after doping is about seven times higher and the OSCs based on P3HT:PCBM improved the PCE from 2.8% to 3.9% owing to increased $J_{sc}$ 16.5 mA cm$^{-2}$ and FF of 38.0% [37]. Another approach includes the addition of commercial surfactants such as Zonyl FS-31, which improves the wettability of the interface between the hydrophobic photoactive layer and the PEDOT:PSS HTL [32]. The fluorination of PEDOT:PSS HTL by fluorinated molecules showed an increased device efficiency [34]. On the other hand, a PSS-free, stable PEDOT HTL was obtained by using solid-state polymerization resulting in robust, stable, and solution-processable OSCs based on PCDTBT:PC$_{71}$BM [38]. Water-soluble polyelectrolyte poly(4-(2,3-dihydrothieno[3,4-b][1,4]dioxin-2-yl-methoxy)-1-butanesulfonic acid) (PEDOT-S), which shows the same PEDOT backbone containing an ethoxyalkylsulfonate branch, showed better performance than conventional PEDOT:PSS layers [36]. PEDOT-sulfonated polyelectrolyte complexes also were tested as anode buffer layer [39]. Different commercial grade of PEDOT:PSS and additive solvent EG were used to form a hybrid PEDOT:PSS (PH 1000:Al 4083) layer tested as HTL and anode electrode for inverted OSCs based on P3HT:PCBM [40].

An OSCs based on PTB7-Th:PC$_{71}$BM was built using a hole transport double layer made of pyridine-based tetrathiafulvalene derivative (TTF-py) on PEDOT:PSS [41]. This modification resulted in an increased short circuit current ($J_{sc}$) of 17.19 mA cm$^{-2}$ and PCE of 9.37%. The anode configuration showed a WF of 5.28 eV for the TTF-py layer resulting in a closer valance band toward the donor material (see Figure 3). PEDOT:PSS/TTF-py had better wetting and enhanced hole mobility, resulting in charge loss reduction and charge recombination suppression. Furthermore, TTF-py molecular structure allowed molecular π-π stacking and form an orderly molecular arrangement for hole transfer. TTF-py modification also improve the device stability retaining 96% of the initial PCE after storing for 28 days by the suppression PEDOT:PSS permeation.
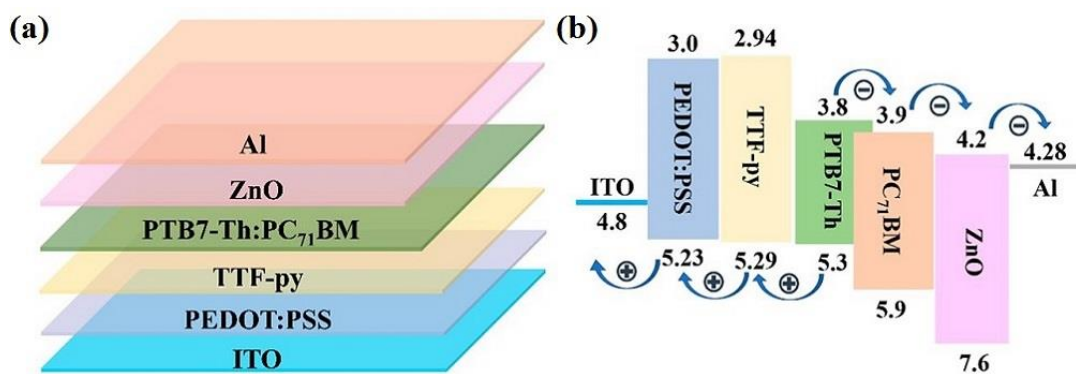
Figure 3. (a) Schematic illustration of device structure ITO/PEDOT.PSS/TTF-py/PTB7-Th:PC$_{71}$BM/ZnO/Al. (b) Schematic diagram of the effect of the device with the TTF-py modified PEDOT:PSS as HTL [41].

Other modifications on PEDOT:PSS have introduced an inorganic transition metal salt, such as nickel formate dihydrate (NFD) to tune the surface free energy ($\gamma_s$) and control the molecular orientation in the BHJ [42]. An enhanced PCE of 10.76% was achieved for the PM6:PC$_{71}$BM-based OSCs. The NFD:PEDOT:PSS HTL had a WF of 5.01 eV that well-matched the donor material and a tuned increased $\gamma_s$ of 68.96 mN m$^{-1}$, which leads to increased FF and J$_{sc}$. Polymeric donor material PM6 preferred face-on molecular orientation. In a BHJ, enhanced molecular stacking is promoted with an increased $\gamma_s$ of PEDOT:PSS induced by NFD. This modification improved the molecular orientation along charge transport direction; thus carrier mobility was enhanced, and the charge recombination was suppressed. The modified HTL was also tested in non-fullerene OSCs based on PM6: IT-4F obtaining enhanced PCE of 14.08% with FF of 78.75%.

Oxoammonium salts (TEMPO$^+$ Br$^-$, 2,2,6,6-tetramethylpiperidine-1-oxoammonium) was tested as a p-type dopant of PEDOT:PSS layers resulting in an enhanced PCE of 16.1% in OSCs based on PM6:Y6 [33]. PEDOT:PSS was further oxidized by oxoammonium salt improving the doping level of PEDOT:PSS. Doped PEDOT:PSS (TEMPO$^+$ Br$^-$) possess higher conductivity and better energy alignment. Metallo phthalocyanines (PC) such as vapor deposited vanadylphthalocyanine (VoPC), NiPC and SnPC were tested as buffer layers with PEDOT:PSS enhancing the efficiency of P3HT:PCBM-based OSCs [43].

PEDOT:PSS:In$_2$S$_3$ was also employed as HTL material for OSCs based on PBDB-T:ITIC and PM6:Y6, these showed an enhanced PCE of 11.22%, and 15.89%, respectively [44]. Improved device performance was observed as a result of increased J$_{sc}$ and FF, and reduced R$_s$ with bimolecular recombination suppression due to partial removal of PSS from the surface. PEDOT

also suffered a benzoic (coil structure)-quinoid (linear structure) transition which delocalized charge carriers enhancing the layer conductivity. Furthermore, device performance stability showed a retained PCE of 36% for modified HTL after 48 hours compared to a non-modified PEDOT:PSS HTL which showed a retained PCE less than 10% . OSCs based on ITO/PEDOT:PSS-Dopamine (DA)/ PM6:Y6/ poly[[2,7-bis(2-ethylhexyl)-1,2,3,6,7,8-hexahydro-1,3,6,8-tetraoxobenzo[lmn] [3,8]phenanthroline-4,9-diyl]-2,5-thiophenediyl[9,9-bis[3'((N,N-dimethyl)-N- ethylammonium)]propyl]-9H-fluorene-2,7-diyl]-2,5-thiophenediyl] (PNDIT-F3N)/Ag showed an increased PCE from 16.01% to 16.55% [45]. DA-doped PEDOT:PSS layer showed an enhanced conductivity ascribed to (i) a more regular stack by the enhanced intermolecular packing of DA:PSS, (ii) an increased WF of 5.14 eV compatible with highest occupied molecular orbital (HOMO) level of PM6 donor polymer, and (iii) enhanced film uniformity. PEDOT:PSS-DA was also tested for devices based on different active layers such as PBDB-T:ITIC, PM6: IDIC, and P3HT:PCBM resulting in improved performances as well.

PEDOT:PSS was also used together with various polymers as HTLs, such as nanoimprinted poly(methylmethacrylate) (PMMA) [46], and conjugated polyelectrolytes e.g., poly[(9,9-bis(4-sulfonatobutyl sodium) fluorene-alt-phenylene)-ran-(4,7-di-2-thienyl-2,1,3-benzothiadiazole-alt-phenylene)] (PSFP-DTBTP), that resulted in a PCE improvement of 13% for PCDTBT:PC$_{71}$BM-based OSCs [47]. For instance, a porous organic polymer, poly(carbazolyl triphenylethylene) derivative (PTPCz) obtained by electropolymerization was used in the HTL PEDOT:PSS/PTPCz for OSCs based on PTB7:PC$_{71}$BM, resulting in an smooth surface morphology, increased WF of 5.23 eV, $J_{sc}$, and FF, reduced series resistance $R_s$ and increased shunt resistance $R_{sh}$ reaching an improved PCE of 8.54% [48]. Electropolymerized polytriphenylcarbazole fluoranthene (p-TPCF) and PEDOT:PSS was used for OSCs based on PTB7-Th:PC$_{71}$BM obtaining enhanced $J_{sc}$, FF, $V_{oc}$ and a PCE of 8.99% [49]. Modification of PEDOT:PSS with a neutral conjugated polymer electrolyte poly[9,9-bis(4′-sulfonatobutyl)fluorene-alt-thiophene] (PFT-D) composite layer improved the device performance (PCE from 7.8% to 8.2%) and the half-lives of PTB7-Th:PC$_{71}$BM-based OSCs [50]. PFT-D molecular dipole screen the attraction between PEDOT and PSS chains as well the –SO$_3^-$ ions of PFT-D acts as a conjugate base of PSS improving current generation. Poly(3-hexylthiophene)-$b$-poly(p-styrenesulfonate) (P3HT$_{50}$-b-PSS$_{23}$) block polymer were incorporated between HTL PEDOT:PSS and the active layer P3HT:PCBM [51]. The OSCs with P3HT-b-PSS interfacial layer improved PCE by 12% due to increased $V_{oc}$ and FF that

compensate for the decreased $J_{sc}$ caused by the light absorption of the P3HT block. The energy level matching was improved, HOMO level of P3HT-b-PSS (-4.68 eV) was higher than P3HT of active layer, which facilitates the hole transport. In addition, P3HT-b-PSS film had a smoother surface than PEDOT:PSS enhancing the interfacial contact, thereby, improving the FF of the device.

Modification of the commonly used PEDOT:PSS with metallic nanoparticles (NPs) contributes with some features as an enhanced localized field and light scattering by the localized surface plasmon resonance (LSPR) that improves the absorption of the active layer. NPs also assist in the charge transport at the interface [52]. NPs are synthetized by different method such as chemical reduction, polyol method [53], and ultrasonochemical synthesis [52, 54]. Hao *et al.* reported a mixed AuNPs (rod, bone-like, cube and spheres shape) doped in PEDOT:PSS HTLs in OSCs based on PTB7:PC$_{71}$BM [55]. Addition of mixed AuNPs generated wide absorption spectra covering from the visible to the near-infrared region and induced an increase of enhancement of internal field in the active layer resulting in improved absorption and enhanced device performance up to 9.26%. AuNPs also contributed to decrease the bulk resistance of PEDOT:PSS. Periodic Ag nanodot (Ag ND) arrays were fabricated by laser interference lithography (LIL) between ITO and PEDOT.PSS layers in OSCs based on PTB7:PC$_{70}$BM (see Figure 4) [56]. This HTL showed improved performance PCE of 10.11%, increased $J_{sc}$ of 23.26 mA/cm$^2$, and enhanced external quantum efficiency (EQE) induced by the plasmonic and light scattering effect. LSPR band matched optimally with the absorption of the photoactive layer, increasing its light-absorption.
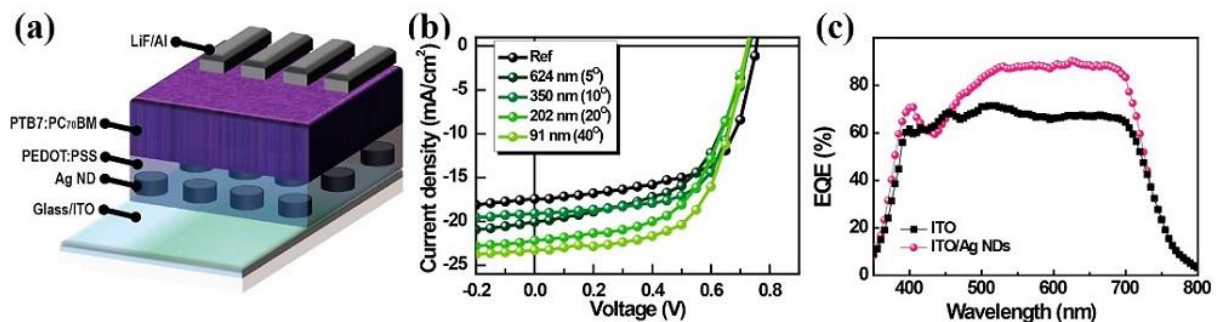


Figure 4. (a) Schematic diagram of an OPV device with Ag NDs. (b) J-V characteristics of devices with and without Ag NDs. (c) EQE spectra of PV devices [56].

AuNPs and AgNPs blended with PEDOT:PSS were used as HTLs in OSCs [57]. Both PEDOT:PSS:NPs showed an enhanced device performance in comparison to pristine PEDOT:PSS with an optimized PCE of 5.65% for PEDOT:PSS:AuNPs HTL in OSCs based on rrP3HT:$PC_{71}$BM. Better devices performance was obtained with NPs because of the surface plasmon effect (at the visible region for AuNPs) that increases the photoabsorption length, scattering and incident light trapping. Segmented silver nanowires (AgNWs) were incorporated in a PEDOT:PSS HTL in OSCs with configuration ITO/PEDOT:PSS:Ag NWs/P3HT:$PC_{61}$BM/ZnO/Al [53]. These OSCs exhibited enhanced device performance with a PCE of 3.3%, increased $J_{sc}$ and FF due to LSPR and optical scattering properties from the AgNWs. Sah *et al.* reported the fabrication of OSCs based on PTB7-Th:$PC_{71}$BM with bimetallic Ag-Au-Ag nanorods (NRs) in PEDOT:PSS HTLs [58]. These devices showed improved performances up to 7.36% by an increased FF and $J_{sc}$. The enhancement was ascribed to an improved charge transport, broad absorption region covering visible to near-infrared region, light scattering induced absorption enhancement, electric field enhancement, and improved EQE by LSPR effect.

Incorporation of copper, a cheaper and more abundant material, as Cu-Au NPs in PEDOT:PSS for OSC based on P3HT:$PC_{61}$BM and PTB7-Th:$PC_{71}$BM showed improved PCEs of 3.63% and 8.48%, respectively [59]. Cu-AuNPs:PEDOT:PSS presented an absorption enhancement by LSPR and light scattering effect. The improved PCE in the device was attributed to an increased $J_{sc}$, higher hole mobility, and reduced $R_s$ obtained with Cu-AuNPs:PEDOT:PSS indicating better hole transport properties. However, the FF decreased compared to pristine PEDOT:PSS HTL, mainly due to an induced charge recombination by the NP doping. Adedeji *et al.* employed copper sulfide NPs in PEDOT:PSS HTLs to fabricate OSCs based on P3HT:$PC_{61}$BM [60]. These devices showed an enhanced PCE of 4.51% (an increase of 115% over the pristine PEDOT:PSS) and good stability, retaining up to 40% of their initial PCEs after 48 h. CuNPs exhibited surface plasmon resonance absorption near-infrared region and induced electric field beneficial to exciton dissociation and photon harvesting. The incorporation of nickel sulphide NPs in PEDOT:PSS layers exhibited an enhanced device performance of 6.03% in OSC based on P3HT:$PC_{61}$BM [52]. An improved photogenerated current was attributed to the effective trapping of light through scattering and improved charge collection. OSCs using NiS NPs in HTL showed reduced $R_s$ indicative of an improved conductivity at the interface, and improved optical transparency enhancing the internal quantum efficiency. Furthermore, the device showed higher hole mobility, thus reduced carrier

recombination and enhanced charge transport. PCE enhancement was ascribed to the LSPR absorption (in the visible and infrared region) and light scattering process.

ZnSTe quantum dots (QDs) incorporated into PEDOT:PSS HTL showed an improved device performance in OSC based on P3HT:PC$_{71}$BM, due to improved mobility and enhanced light absorption attributed to surface plasmon resonance [61]. Zhang *et al.* reported OSCs based on PTB7-Th:PC$_{71}$BM and PM6:IT-4F with high PCEs of 9.11% and 12.81%, respectively, by the insertion of black phosphorous quantum dots (BPQDs) on PEDOT:PSS [62]. BPQDs is a 2D p-type semiconductor, which inside the device formed a cascade band structure between the anode and active layer. The valance band of BPQDs (-4.92 eV) was higher than the valance band of donor polymers PTB7-Th (-5.24 eV) and PM6 (-5.5 eV), providing enough driving force for the hole injection from the active layer to the BPQDs layer (see Figure 5. The energy level diagrams of the components in the devices [62].Figure 5). The increased efficiency in devices with BPQDs interfacial layer was attributed to an increased J$_{sc}$ and FF due to excellent hole mobility in BPQDs and better energy alignment in the device, indicating improved charge extraction and exciton dissociation.
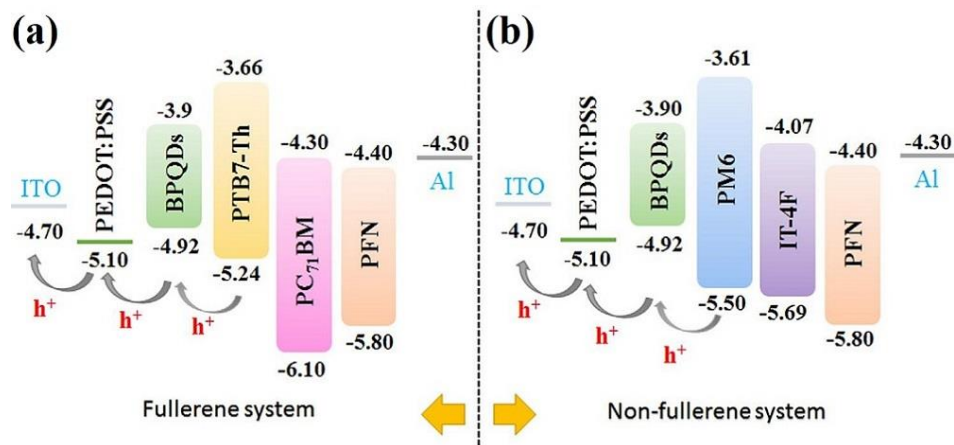


Figure 5. The energy level diagrams of the components in the devices [62].

Other metal NPs incorporated in PEDOT:PSS involve Al micro-stars [63], Al NPs [64], and Au NPs [65–67], gold nanorods (Au NRs) [68], and Au QDs [69].

Up-conversion NP process converts low-energy photons into high-energy photons (in the absorption region of organic polymers) to enhance the optical-to-electrical conversion performance [70]. Mei *et al.* incorporated sodium yttrium fluoride (β-NaYF$_4$):Er$^{3+}$,Yb$^{3+}$ up-

conversion NPs into PEDOT:PSS HTLs in OSCs based on P3HT:PC$_{61}$BM resulting in enhanced J$_{sc}$ and PCE of 3.02% [71]. These results were ascribed to light scattering and photoluminescence (PL) emission from up-conversion NPs. The silver-zinc bimetallic NPs layer was incorporated between the PEDOT:PSS HTL and the photoactive layer of P3HT:PCBM [72]. The OSCs exhibited an improved PCE of 3.6%, which is 90% higher than the reference device. This was attributed to LSPR of the Ag:Zn NPs which enhanced the optical absorption and charge carriers collection. Another modification to PEDOT:PSS was reported by Michalska *et al.* using wet ultra-sonochemical synthetized titanium dioxide TiO$_2$ anatase decorated with Ag NPs [54]. TiO$_2$/Ag solution was added to PEDOT:PSS HTL in OSCs based on P3HT:PCBM showing an improved PCE of 2.07%. Gold nanoparticles (Au NPs) on PEDOT:PSS in vacuum-free OSCs improved the device performance resulting from the increased J$_{sc}$ [73]. The absorption of the active layer and the device PCE was enhanced, especially by Au nanorods' presence.

Many studies have been focused on improving the performance of PEDOT:PSS HTL by addressing the acidic and hygroscopic nature of PEDOT:PSS that affects the stability and efficiency of the photovoltaic devices. Incorporating metal oxides (MO) can enhances the stability, efficiency, and electron blocking properties of the HTL. Among these MOs that have been incorporated in PEDOT:PSS are vanadium oxides (V$_2$O$_5$) [74, 75], sol-gel synthesized VO$_x$ [76], continuous spray pyrolyzed synthesized molybdenum oxide (MoO$_3$) [77], and tungsten oxide (WO) [78, 79].

Spin-coated V$_2$O$_5$ nanowires, prepared by hydrothermal method, on PEDOT:PSS as HTL of OSCs based on P3HT:PCBM showed increased device parameters, improved V$_{oc}$ and FF [80]. The PCE improved a 15.58% in comparison with PEDOT:PSS reference cell. The lowest unoccupied molecular orbital (LUMO) level of V$_2$O$_5$ (2.4 eV) is higher than P3HT LUMO, thus better electron blocking than pristine PEDOT:PSS (see Figure 6 (b)). Modified HTL had increased incident light paths by reflection and refraction caused by V$_2$O$_5$ nanowires.
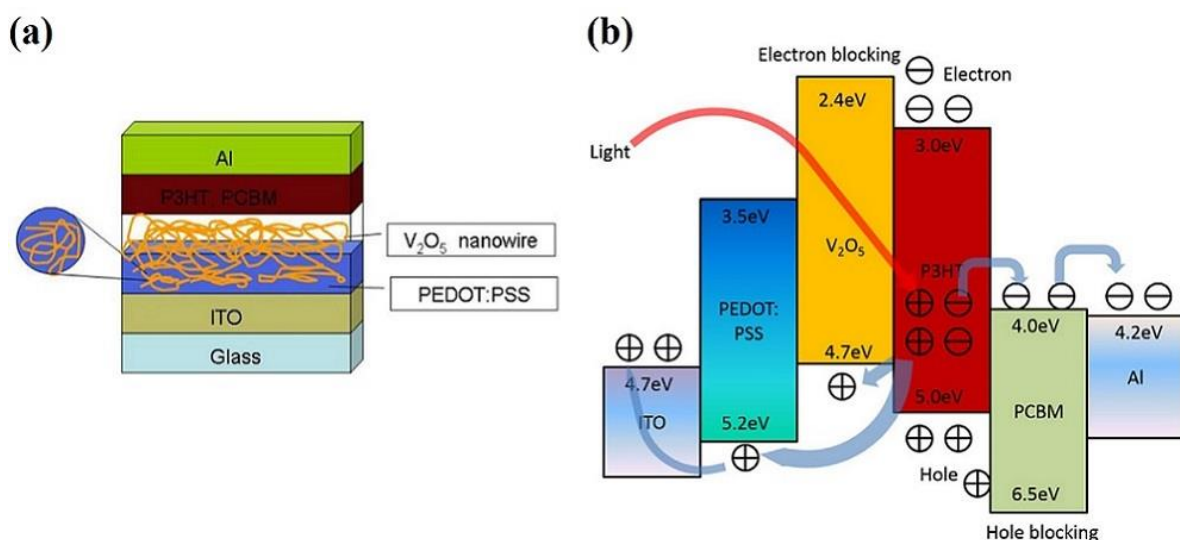
Figure 6. (a) Structure of polymer photovoltaic cell based on PEDOT:PSS/V$_2$O$_5$ HTL. (b) Schematic energy level alignment of V$_2$O$_5$ over PEDOT:PSS layer [80].

Li *et al.* reported a PCE of 9.44% for OSCs with V$_2$O$_5$:PEDOT:PSS as HTL due to an enhanced J$_{sc}$ and FF, smaller R$_s$, and larger R$_{sh}$ [81]. The incorporation of V$_2$O$_5$ offered an effective path for exciton extraction and suppress charge recombination reflected by a larger hole mobility and a higher conductivity. The composite HTL surface was uniform and smooth related to V$_2$O$_5$ nanoparticles filling the pinholes in PEDOT:PSS. Furthermore, better wetting and physical contact were obtained between the photoactive layer and the HTL as well as enhanced crystallinity of the active layer.

Molybdenum oxide (MoO$_x$) NPs/PEDOT:PSS HTLs were blade coated in inverted OSCs based on PTB7-Th:PC$_{60}$BM resulting in enhanced PCE of 7.4% and increased FF [82]. The modification of PEDOT:PSS with MoO$_3$ mitigated the degradation of non-fullerene OSCs based on PM6:IT-4F by suppressing the interfacial reaction between PEDOT:PSS and IT-4F [83]. MoO$_3$-PEDOT:PSS hybrid HTL improved the device's operational stability which was five times longer than reference devices. The hybrid HTL also improved the hole mobility favoring the charge extraction. Zinc oxide doped single carbon nanotubes (CNT) were incorporated in PEDOT:PSS as anode buffer layer (ZnO:CNT/PEDOT:PSS), showing excellent transmittance and a smooth morphology [84]. P3HT:PCBM based cell with an HTL containing 2.5% ZnO:CNT showed an improved PCE of 4.1%, enhanced J$_{sc}$ and FF, and reduced R$_s$. CNT provided surface homogeneity, and ZnO prevented humidity uptake. The device parameters decreased at a slower rate than PEDOT:PSS devices under a nitrogen environment. Zheng *et al.* fabricated fullerene-free OSCs with tungsten oxide WO$_x$ NPs in

14

PEDOT:PSS as HTL [78]. The system architecture ITO/WO$_x$:PEDOT:PSS/PM6:IT-4F/PFN-Br/Al achieved a high FF of 80.79%, consequently an enhanced PCE of 14.57%. A more balanced hole and electron mobility of BHJ on WO$_x$:PEDOT:PSS measured as a ratio $\mu_e/\mu_h$ of 0.88 which contributed to increased FF. The longer lifetime of carriers and faster extract time of WO$_x$:PEDOT:PSS also benefited the device parameters. WO$_3$/PEDOT:PSS bilayer was used as HTL in inverted SMD2: ITIC-Th based OSCs [79]. An optimized cell achieved a high PCE of 10.3%, with enhanced J$_{sc}$, V$_{oc}$, and FF. The WO$_3$/PEDOT:PSS device presented increased R$_{sh}$ and decreased R$_s$ by a well-matched energy level alignment, high hole mobility, a more balanced charge carrier transport, and increased photostability. Furthermore, flexible inverted OSC modules were fabricated by slot-die coating achieving a PCE of 5,25% and a power output of 419.6 mW. A layer of hydrogen molybdenum bronze (H$_x$MoO$_3$) with PEDOT:PSS layer was also used in an all solution-processed non-fullerene OSCs based on PM6:IDIC:Y6 [85]. Phosphomolybdic acid (PMA) in PEDOT:PSS layers were tested in different organic fullerene-based OSC showing good performances [86].

Graphene oxide (GO), a two-dimensional carbon material, has also been investigated to modified PEDOT:PSS as hole transport materials in different OSCs. Oleyamine-functionalized GO/PEDOT:PSS layer on PBDB-T:ITIC [87], PEDOT:PSS treated with GO layers on PTB7:PC$_{71}$BM devices [88], on P3HT:PC$_{60}$BM devices [89], on P3HT:PCBM devices [90], on inverted P3HT:PCBM OSCs [91], on inverted P3HT:PC$_{71}$BM OSCs [92], and reduced GO-germanium QDs modified PEDOT:PSS on P3HT:PCBM [93]. Raj *et al.* reported the fabrication of PTB7:PC$_{70}$BM-based OSCs with PEDOT:PSS:GO resulting in enhanced PCE of 7.68% [94]. The modified HTL showed a fine fiber-like structure that improved the conductivity. GO showed to increase the device resistance degradation. GO is generally prepared by variations of the Hummers method using graphite powder as starting material [95], [96]. PEDOT:PSS:GO was also tested on P3HT:PC$_{61}$BM based OSCs showing an increased J$_{sc}$, FF, and a 14% higher PCE than a reference device [97]. GO in the HTL reduced the HOMO-LUMO gap and the R$_s$, improved the hole mobility and the energy level matching. A double-decked GO/PEDOT:PSS HTL in PCDTBT:PC$_{71}$BM based OSCs was reported by Rafique *et al.* [98]. The modified HTL provided a better hole extraction and transportation by a suitable WF of GO (4.9 eV) and PEDOT:PSS (5.1 eV) that well-matched energy levels (see Figure 7 (a) and (b)). This device showed an improved PCE of 4.28% ascribed to an increased charge carriers mobility, J$_{sc}$, V$_{oc}$, and FF, and a reduced R$_s$. Besides, better stability than

PEDOT:PSS was reached, since GO served as a barrier that protected ITO corrosion due to the acidic nature of PEDOT:PSS (see Figure 7 (c)). Similarly, improved photovoltaic stability was achieved with GO/PEDOT:PSS HTLs in P3HT:PC$_{60}$BM devices [99]. This device showed an increased R$_{sh}$ and a decreased R$_s$, which facilitate the hole transportation. The composite HTL was smooth and uniform, contributing to an improved device performance with a PCE of 4.82%. Nitrogen-doped graphene quantum dots (nGQDs) were blended with PEDOT:PSS HTLs in PTB7:PC$_{71}$BM based OSCs resulting in an enhanced PCE of 8.5% [100]. The modified HTL improved the charge carrier transport, increased the hole mobility, and suppressed charge recombination. The nitrogen doping led to a high content of quaternary nitrogen, enhancing the electrical conductivity of GQDs. UV-ozone (UVO) treated GO/PEDOT:PSS bilayer in OSCs based on PCDTBT:PC$_{71}$BM presented an improved PCE of 5.24% [101]. An increased J$_{sc}$, V$_{oc}$, and FF obtained in the cells using the modified HTL and improved ambient stability retaining above 90% of initial PCE after 240 h. The enhanced conductivity was ascribed to the reduction of oxygen content in GO after UVO treatment. Electrochemically synthesized graphene was incorporated on PEDOT:PSS HTLs in OSC based on P3HT:PCBM resulting in a 66.7% increased PCE compared to a reference device [102].
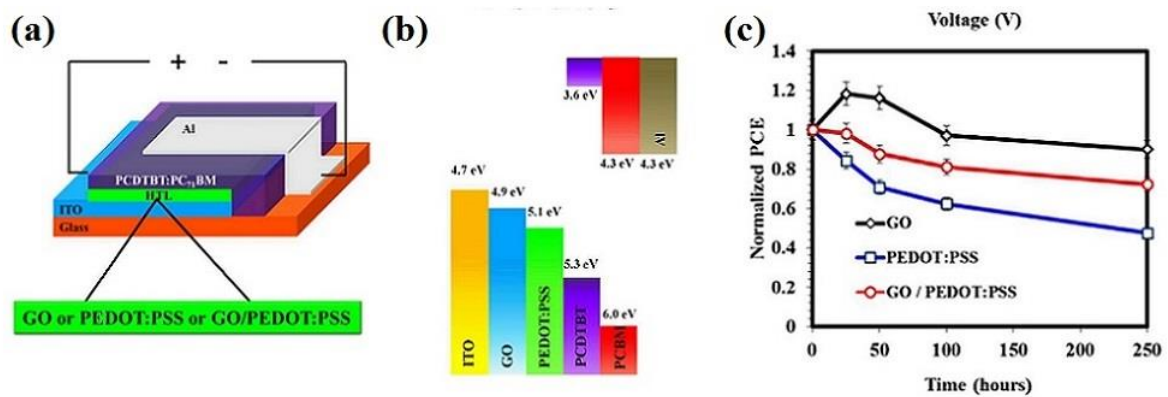


Figure 7. (a) Scheme of the OSCs with GO, PEDOT:PSS HTLs. (b) Energy band diagram of material used. (c) Stability test of OSCs over 250h [98].

Other modifications on PEDOT:PSS have also been reported with a graphene analog, the two-dimensional transition metal dichalcogenides. For instance, hybrid PEDOT:PSS/WS$_2$ was incorporated as HTL in OSCs [103]. PEDOT:PSS worked as an effective exfoliating agent to WS$_2$ 2D structure. The photovoltaic device based on P3HT:PC$_{61}$BM and PTB7-Th:PC$_{71}$BM exhibited enhanced PCE of 3.07 and 7.24%, respectively, attributed to increased J$_{sc}$ and FF as

well as to enhanced hole mobility and enhanced conductivity of PEDOT:PSS/WS$_2$ layer. Besides, PEDOT:PSS/WS$_2$-based OSCs had improved stability, it kept 77.3% of initial PCE after 36 days. Koo *et al.* fabricated PTB7:PC$_{71}$BM based OSCs with tungsten diselenide (WSe$_2$) / PEDOT:PSS HTLs (Figure 8(a)) showing an enhanced PCE of 8.5 [104]. The composite HTL exhibited a homogeneous film formation. WSe$_2$ negative surface-induced the segregation of PEDOT and PSS, which enhanced the layer conductivity. Furthermore, photoluminescence peak intensity decreased, indicating diminished recombination (see Figure 8 b). Thus, PEDOT:PSS-WSe$_2$ showed improved hole transport ability and a better charge extraction than the reference device. Oleyamine-functionalized molybdenum disulfide MoS$_2$ has also been reported in the modification of PEDOT:PSS HTLs [105].
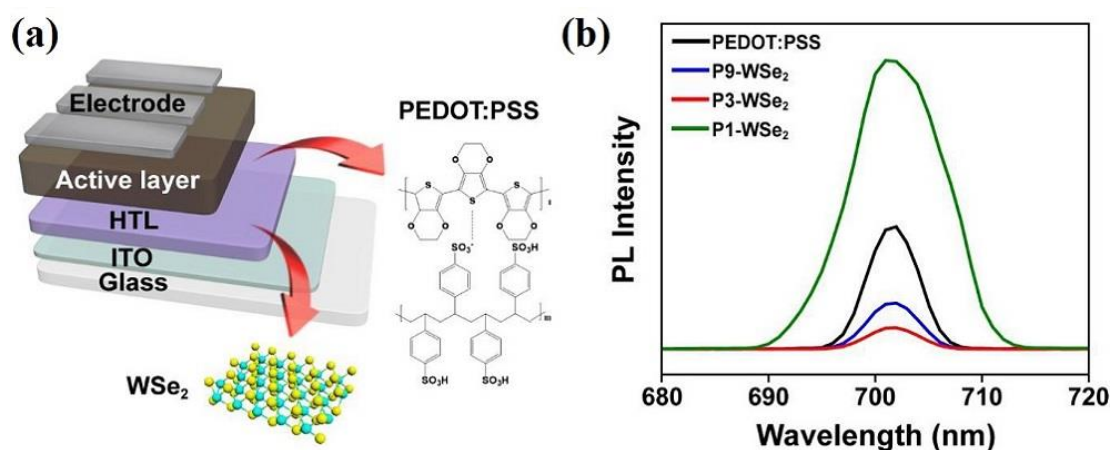


Figure 8. (a) Device structure with WSe$_2$ -PEDOT:PSS HTL and (b) Steady state PL spectra measured from structure of glass/PEDOT:PSS or P- WSe$_2$/PTB7:PC$_{71}$BM [104].

Boronic acid functionalized multi-walled CNs (bf-MWCNTs) doped PEDOT:PSS HTLs showed excellent hole mobility and electrical conductivity [106]. The OSC with PEDOT:PSS:bf-MWCNTs showed reduced R$_s$ and increased R$_{sh}$ exhibiting excellent hole collectivity. An enhanced of 28% PCE for PCDTBT:PC$_{71}$BM based OSC was attributed to an increased J$_{sc}$ and FF. PL intensity of HTL doped with bf-MWCNTs was reduced, indicating an enhancement in charge transport from the active layer. The WF increased to 5.39 eV that well-matched with the HOMO energy level of PCDTBT. Graphitic carbon nitrile (g-C$_3$N$_4$) was used as a secondary dopant for PEDOT:PSS in OSCs based on PM6:Y6, leading to an improved PCE of 16.38% [107]. The g-C$_3$N$_4$:PEDOT:PSS HTL showed a higher conductivity, an improved charge transport and a suppressed charge recombination. This modified HTL had

increased hole mobility leading to more balanced charge transport. The g-$C_3N_4$ insulated the PSS moiety, so the conducting PEDOT chain was exposed. Zhang *et al.* reported unzipped single-walled carbon nanotubes (uSWNT) / PEDOT:PSS double-decked HTLs in PM6:IT-4F based OSCs [108]. Optimized HTLs with 0.1 mg mL$^{-1}$ uSWNTs resulted in improved PCE of 14.60% attributed to an increased $J_{sc}$ of 23.39 mA cm$^{-2}$ and FF of 73,17%. Moreover, the modified HTL exhibited increased conductivity and increased hole transport efficiency.

Two-dimensional titanium carbide ($Ti_3C_2T_x$) bilayer was incorporated into PEDOT:PSS HTLs in non-fullerene PBDB-T:ITIC, and PM6:Y6 OSCs [109]. This bilayer enhanced the conductivity of PEDOT:PSS by a reduced coulombic attraction between PEDOT and PSS, causing the conformational transition of PEDOT from the coil to linear structures. The HTL roughness increased upon $Ti_3C_2T_x$ incorporation, which enlarged the contact area between HTL and the photoactive layer. The hole mobility increased as a result of the interconnected conducting network between PEDOT and $Ti_3C_2T_x$. The PL peak was reduced, indicating improved hole transmission. As a consequence, the PCE of devices improved to 11.02% and 14.55% for PBDB-T:ITIC and PM6:Y6 based OSCs, respectively. Moreover, PEDOT:PSS/$Ti_3C_2T_x$ HTLs enhanced the nitrogen atmosphere's long-term stability remaining 79.67% of the initial PCE after 300 h.

### 2.1.2 Other conjugated polymers and composites

Another approach aims to replace the use of PEDOT:PSS with different conjugated polymers. Conjugated polyelectrolytes (CPE) composed of conjugated backbone and side chains containing ionic groups have been used as HTL materials due to their good solubility in polar solvents. The structure of these used as HTL are shown in Figure 9. For example, thiophene based CPE, poly[1,4-bis(4-sulfonatobutoxy)benzene-thiophene] PhNa-1T self-doped in a neutral state achieves an increased WF of 5.21 eV resulting in PCEs of 9.89% and 8.38% for ITO/PhNa-1T/PTB7-Th:PC$_{71}$BM/fullerene derivative (bis-C$_{60}$)/Ag and ITO/PhNa-1T/PTB7:PC$_{71}$BM/TiO$_2$/Al cells, respectively [110]. The enhanced device performance was ascribed to improved interfacial properties, a high WF, and a smoother surface resulting in a favorable contact, improved charge extraction, and an efficient hole collection. Similarly, PhNa-DTBT is based on a weakly electron-donating 2-phenyl thiophene, an electron-acceptor 2,1,3-benzothiadiazole and sulfonate sodium salt as an ionic functional group, was used in OSC based on PTB7-Th:PC71BM, reaching a PCE of 9.29% [111]. PhNa-DTBT shows a high

electrical conductivity, improved $J_{sc}$ and FF, and high WF (5.39 eV). The device also shows improved stability with a retained PCE of ca. 40% after 96 h. A pH neutral self-doped polymer based on phenyl and thienyl units, poly[2,6-(4,4-bis-(propane-1-sulfonate sodium)-4H-cyclopenta[2,1-b ;3,4-b' ]dithiophene)-alt-(4,4′-biphenyl)] (PCP-Na) was used as HTL for PBDT-TS1:PC$_{71}$BM-based OSCs [112]. PCP-Na had a suitable HOMO level, smoother surface and a high electrical conductivity by the presence of polaronic states (radical cations). PCP-Na exhibited appreciable hole collection and charge transport properties. The photovoltaic device using PCP-Na showed a PCE of 9.89% that resulted mainly from an enhanced FF. Following the same line, pH neutral poly[9,9-bis(4′-sulfonatobutyl)fluorene-alt-selenophene] (PFSe) (see structure in Figure 9) was used as HTL in OSCs with architecture ITO/PFSe/PTB7:PC$_{71}$BM/PFN/Al exhibiting a PCE of 7.2% [113]. An increased $J_{sc}$ and FF was ascribed to a strong dipole moment at the interface. A WF of 5.15 eV of PFSe assured a good ohmic contact and a better matching energy level. Moreover, the air stability of the cell was improved by the neutral nature of HTL polymer. Xu *et al.* reported a pH-neutral conjugated polyelectrolyte, 3,4-dithia-7H-cyclopenta[a]pentalene and thienyl units (PCPDT) used in OSCs based on PTB7-Th:PC$_{71}$BM with a PCE of 9.3% [114]. Improved device performance by using PCPDT HTL was attributed mainly to a reduced leakage current and $R_s$. A tuned WF of -4.87 eV, enhanced transmittance, improved and homogeneous mobility of HTL was related to the strong p-type self-doped nature of this HTL. Moreover, the hole layer showed improved interface compatibility, evidenced by the reduced surface energy (30.7 mN m$^{-1}$). The use of PCPDT-K HTL in OSC based on P3HT:PCBM showed improved device performance (PCE of 3.11%), increased $J_{sc}$, reduce $R_s$, a smooth surface, and better stability than a PEDOT:PSS reference device [115]. PCPDffPhSO$_3$K a neutral CPE based on 3,4-dithia-7H-cyclopenta[a]pentalene and 1,4-difluorobenzene units was used as HTL for OSCs ITO/HTL/PTB7-Th:PC$_{71}$BM/PFN/Al OSCs resulting in PCE of 9.5% [116]. The self-doping effect in PCPDffPhSO$_3$K improved its conductivity. A WF around -5.18 eV ensured a better energy level alignment achieving a higher $V_{oc}$, $J_{sc}$, and hole mobility. Lee *et al.* utilized poly[9,9-bis(4'-sulfonatobutyl)fluorene-alt-thieno[3,2-b]thiophene] (PFtT-D) HTLs showing a PCE of 8.3% for OSCs based on PTB7-Th:PC$_{71}$BM [117]. The WF of the modified electrode with PFtT-D was 5.19 eV that resulted in superior ohmic contact due to well-matched energy levels facilitating the hole transportation. The modification of WF is attributed to the molecular dipole orientations. The device showed an improved lifetime because of the neutral nature of CPE; the PCE slowly decreased with a half-live of 153 h.

PCPDTK$_{0.50}$H$_{0.50}$-TT another neutral self-doped CPE was used as HTL for the OSCs based on PM6:Y6:PC$_{71}$BM [118]. Potassium ions were exchanged to protons through ion-exchange chromatography using acid sulfonated polystyrene resin. PCPDTK$_{0.50}$H$_{0.50}$-TT HTL had a higher WF and increased mobility, and it also exhibited a higher hole extraction efficiency. The device performance with this HTL was improved with a PCE of 16.3%. The V$_{oc}$ increased due to the improved hole mobility, and the J$_{sc}$ and FF were also improved ascribed to reduced carrier recombination and reduced bulk resistance. The device showed improved stability, the PCE was retained by a longer time than with PEDOT:PSS. These OSCs showed is compatible with large-area printing technique. OSCs with an area of 1.0 cm$^2$ prepared by wire-bar coating obtained a PCE greater than 10%.
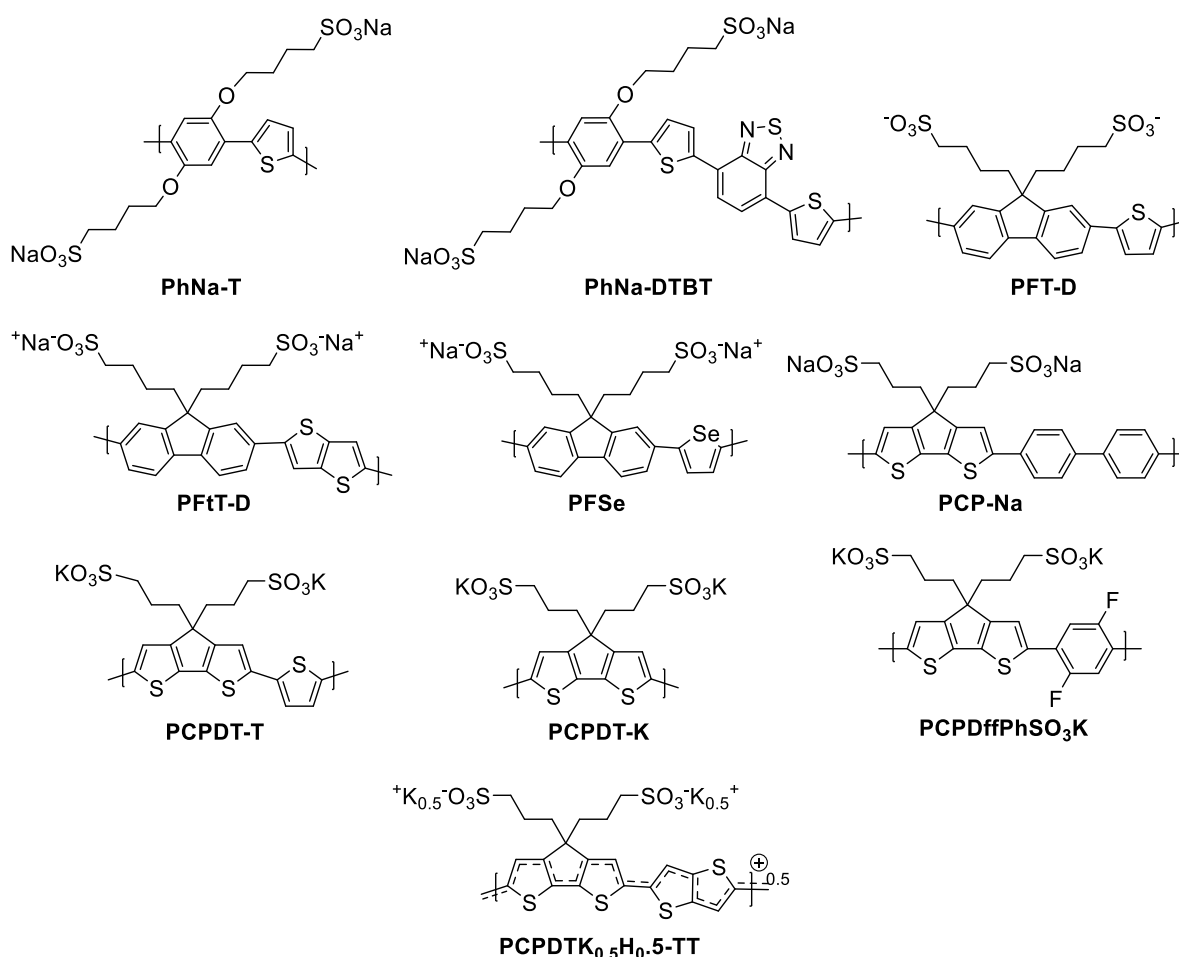
Figure 9. Molecular structure of some conjugated polyelectrolytes for HTL.

The structure of some conjugated polymers used as HTL for OSCs are shown in Figure 11. A HTL nanocomposite made of fluorene conjugated polymer, poly[(9,9-bis(3′-(N,N-

dimethylamino)propyl)-2,7-fluorene)-alt-2,7-(9,9-dioctyl)fluorene] and nickel oxide (PFN/NiO$_x$) showed a power conversion efficiency of 6.2% in OSCs based on PBDTTBO-C$_8$:PC$_{71}$BM (see Figure 10 (a), (b)) [119]. The device performance improvement was related to the interaction between PFN and NiO$_x$, p-doping effect in NiO$_x$ improved FF, and good energy alignment. A blend of 5,6-difluorobenzothiadiazole conjugated polymer and metal oxide (Cu$_2$O/FBT-TH4) gave a PCE of 9.56% for OSCs based on PffBT4T-2OD:PC$_{71}$BM [120]. A better charge transfer properties and stability were determined maintaining the 75% of the original PCE up to 30 days that was attributed to the hydrophobic character of the HTL. Poly(3,4-dimethoxythiophene) (PDMT) deposited via oxidative chemical vapor deposition was also used as hole transport materials in OSCs [121].
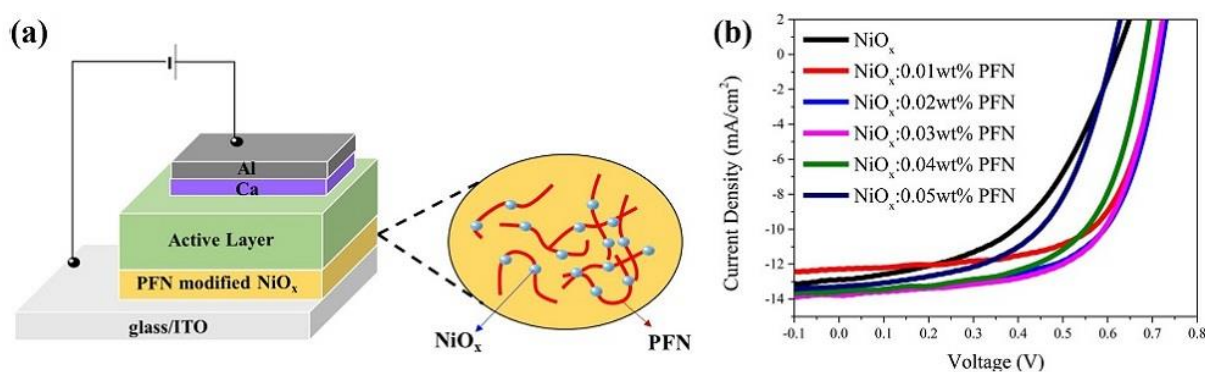


Figure 10. (a) Device structure with HTL of PFN modified NiO$_x$, (b) J-V curves of ITO/HTL/PBDTTBO-C$_8$:PC$_{71}$BM/Ca/Al devices [119].

Awada *et al.* fabricated OSCs based on hydrophobic triethoxysilane terminated poly(3-hexylthiophene) (P3HT-Si) (Figure 11) HTLs exhibiting a slightly enhanced device stability [122]. Some other polymers and composites used as hole transport layers include P3HT:SWCNTs [123], and polyaniline / gold and silver NPs composite (Au$_{10}$Ag$_{10}$PANI), which showed improved conductivity, improved WF, and increased PCE in P3HT:PCBM based OSCs [124]. The interconnected network of grafted carbon nanotubes, polythiophenic agents, and conjugated PANI bottlebrushes (CNT-g-PDDT:P3ThEt-g-PANI) were used as HTL in OSCs based on PBDT-DTNT:PC$_{61}$BM showing smooth morphology, low sheet resistance, and a PCE of 5.65% [125]. A network of carbon nanotubes and polythiophene/polyaniline bottlebrushes (CNT:P3ThEt-g-PANI) was tested as HTL in OSCs based on P3HT:PC$_{71}$BM reaching an improved PCE of 5.30% [126]. Another approach

involves the use of low acidic water-stable PSS doped PANI as HTL based on P3HT: ICBA OSCs [127]. PANI:PSS layer presented a well-matched WF, higher conductivity, transmittance around 90% and led to PCE of 4.5%. Additionally, PANI:PSS HTL had also been tested for indoor photovoltaics [128, 129]. The OSCs based on P3HT:ICBA showed a lower PCE than a device using PEDOT:PSS, but possessed better stability over 1176 hours, retaining 39% of its initial PCE. PANI was also tested with graphene oxide (GO) as an acid-free composite HTL in OSCs based on P3HT:PCBM and PCDTBT:PC$_{71}$BM resulting in optimized performance for the nanocomposite with a GO loading of 7.3 wt% [130]. A hole transporting bilayer of copper(I) thiocyanate and poly[(9,9-dioctylfluorenyl-2,7-diyl)-alt-(4,4'-(N-(4-butylphenyl)))] (CuSCN/TFB) was tested in OSCs based on non-fullerene PM6:Y6 and fullerene PTB7-Th:PC$_{71}$BM by Dong *et al.* [131]. Better photovoltaic performance with CuSCN/TFB bilayer than with pristine CuSCN HTL was related to enhanced J$_{sc}$ and FF. The decreased roughness and increased contact angle of the bilayer favored the interfacial contact of the HTL and the active layer, leading to better energy matching and device performance (up to 15.10%). Furthermore, the CuSCN/TFB based device presented improved hole mobility, higher exciton dissociation efficiency and lower recombination loss which contributed to its enhanced charge transportation and extraction, and exciton dissociation.
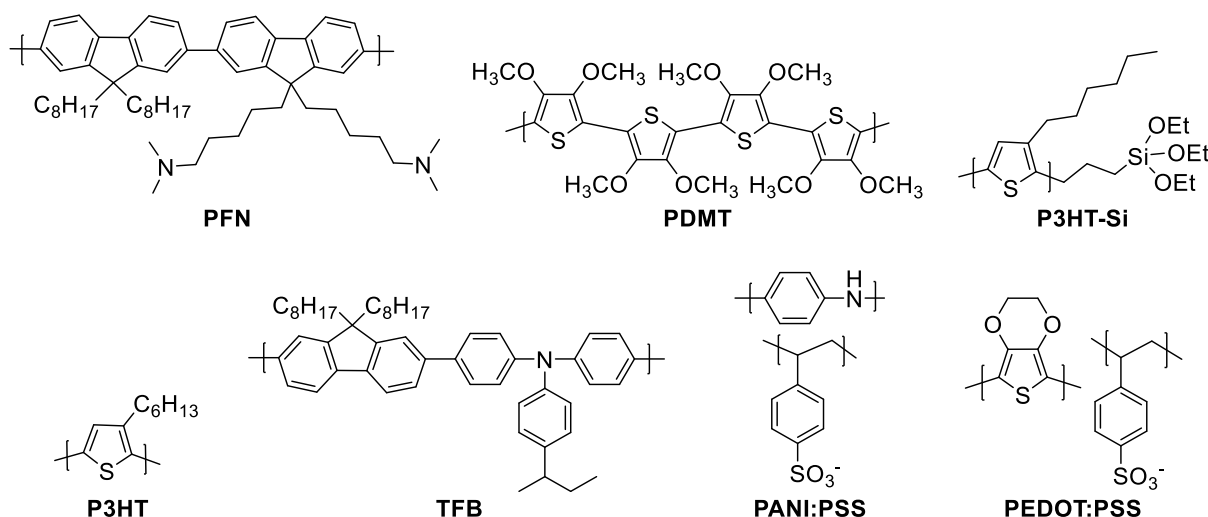


Figure 11. Molecular structures of some conjugated polymers for HTLs.

Table 1 summarizes the parameters of some OSCs with conducting polymers used as HTLs.

Table 1. Device characteristics of some representative OSCs with different conducting polymers as HTLs.

| Anode configuration | Deposition technique | Remaining architecture cell | $V_{OC}$ (V) | $J_{SC}$ (mA cm$^{-2}$) | FF (%) | PCE (%) | Ref. |
|---|---|---|---|---|---|---|---|
| PEDOT modifications | | | | | | | |
| PEDOT:PSS/Ag | slot-die-coating | flextrode/P3HT:O-IDTBR | 0.71 | 8.07 | 67.3 | 3.80 | [29] |
| ITO/PEDOT:PSS | spin coating | P3HTN:PEG-C60/Cs$_2$CO$_3$/Ag | 1.31 | 0.55 | 33.4 | 0.24 | [30] |
| ITO/PEDOT:PSS/IPA | spin coating | P3HT:PC$_{71}$BM/Al | 0.60 | 11.76 | 54.9 | 3.87 | [31] |
| PEDOT:PSS-FS-31/Ag | slot-die coating | ITO/ZnO/P3HT:ICBA | 0.80 | 10.55 | 48.0 | 4.06 | [32] |
| ITO/PEDOT:PSS:TEMPO$^+$Br$^-$ | spin coating | PM6:Y6/PFN-Br/Ag | 0.82 | 27.18 | 72.6 | 16.10 | [33] |
| ITO/PEDOT:PSS:FOS | spin coating | PTB7:PC$_{70}$BM/Ca/Al | 0.70 | 16.94 | 69.3 | 8.26 | [34] |
| ITO/PEDOT:GSL | spin casting | PTB7-Th:PC$_{71}$BM/PFN/Al | 0.77 | 15.82 | 68.7 | 8.47 | [35] |
| ITO/PEDOT-S | spin coating | P3TI:PC$_{71}$BM/LiF/Al | 0.73 | 12.80 | 72.0 | 6.70 | [36] |
| Ag/ssp-PEDOT | spin coating | PCDTBT:PC$_{71}$BM/Al | 0.46 | 9.30 | 38.9 | 1.70 | [38] |
| ITO/PEDOT-polyelectrolyte | electrodeposition | P3HT:PCBM/LiF/Al | 0.51 | 6.70 | 31.6 | 1.93 | [39] |
| PEDOT:PSS(PH 1000:Al 4083:EG) | spin coating | ITO/ZnO/P3HT:PCBM | 0.58 | 6.91 | 51.2 | 2.04 | [40] |
| ITO/PEDOT:PSS/TTF-py | spin coating | PTB7-Th:PC$_{71}$BM/ZnO/Al | 0.79 | 17.19 | 70.6 | 9.37 | [41] |
| ITO/PSS:PEDOT:PSS | spin coating | PDCBT:PC$_{71}$BM/PFN-Br/Al | 0.83 | 12.44 | 77.2 | 7.97 | [42] |
| ITO/NiFD:PEDOT:PSS | | PM6:PC$_{71}$BM/PFN-Br/Al | 0.98 | 13.82 | 79.4 | 10.76 | |
| ITO/PEDOT:PSS:VoPC | spin casting/ thermal evaporation | P3HT:PCBM/Al | 0.60 | 14.80 | 53.0 | 3.61 | [43] |
| ITO/PEDOT:PSS:a-In$_2$Se$_3$ | spin coating | PBDB-T:ITIC/PFN-Br/Al | 0.91 | 17.31 | 71.1 | 11.22 | [44] |
| | | PM6:Y6/PFN-Br/Al | 0.84 | 25.47 | 74.5 | 15.89 | |
| ITO/PEDOT:PSS-DA | spin coating | PM6:Y6/PNDIT-F3N/Ag | 0.84 | 25.52 | 77.1 | 16.55 | [45] |
| FTO/PMMA/PEDOT:PSS | nanoimprinting/ spin coating | PTB7:PC$_{70}$BM/TiOx/Al | 0.73 | 16.30 | 68.2 | 8.12 | [46] |
| ITO/PEDOT:PSS:PSFP-DTBTP | spin coating | PCDTBT:PC$_{71}$BM/(Ca)/Al | 0.88 | 9.46 | 66.3 | 5.26 | [47] |
| ITO/PEDOT:PSS/PTPCz | spin coating/ electrodeposition | PTB7:PC$_{71}$BM/Ca/Al | 0.74 | 16.23 | 71.1 | 8.54 | [48] |
| ITO/PEDOT:PSS/p-TPCF | electrochemical cyclic voltammetry | PTB7-Th:PC$_{71}$BM/PFN-Br/Al | 0.80 | 16.98 | 66.2 | 8.99 | [49] |
| ITO/PEDOT:PSS+PFT-D | spin coating | PTB7-Th:PC7$_1$BM/PFN/Al | 0.77 | 14.90 | 71.3 | 8.20 | [50] |

| | | | | | | | |
|---|---|---|---|---|---|---|---|
| ITO/PEDOT:PSS/P3HT-b-PSS | spin casting | P3HT:PCBM/Al | 0.60 | 7.47 | 63.9 | 2.80 | [51] |
| PEDOT:PSS with NPs | | | | | | | |
| ITO/PEDOT:PSS-NiS | spin coating | P3HT:PC$_{61}$BM/LiF/Al | 0.58 | 18.65 | 55.9 | 6.03 | [52] |
| ITO/PEDOT:PSS:Ag NWs | spin coating | P3HT:PC$_{61}$BM/ZnO/Al | 0.60 | 9.95 | 55.8 | 3.30 | [53] |
| ITO/PEDOT:PSS:TiO$_2$/n-Ag | spin casting | P3HT:PCBM/Al | 0.61 | 5.94 | 57.0 | 2.07 | [54] |
| ITO/PEDOT:PSS+Au NPs | spin coating | PTB7:PC$_{71}$BM/Al | 0.74 | 18.30 | 68.0 | 9.26 | [55] |
| ITO/Ag ND/PEDOT:PSS | LIL/ spin coating | PTB7:PC$_{70}$BM/LiF/Al | 0.73 | 23.26 | 61.0 | 10.11 | [56] |
| ITO/PEDOT:PSS+Au NPs | spin coating | rrP3HT:PC$_{61}$BM/BCP/LiF/Al | 0.59 | 13.90 | 62.0 | 4.99 | [57] |
| | | rrP3HT:PC$_{71}$BM/BCP/LiF/Al | 0.58 | 16.10 | 61.0 | 5.65 | |
| | | rrP3HT:PC$_{61}$BM/BCP/LiF/Al | 0.58 | 13.10 | 62.0 | 4.94 | |
| | | rrP3HT:PC$_{71}$BM/BCP/LiF/Al | 0.58 | 14.70 | 61.0 | 5.29 | |
| ITO/PEDOT:PSS:Ag-Au-Au NRs | spin coating | P3HT:PC$_{61}$BM/Ca/Al | 0.62 | 10.11 | 69.0 | 4.34 | [58] |
| | | PTB7:PC$_{71}$BM/Ca/Al | 0.73 | 16.87 | 60.0 | 7.36 | |
| ITO/PEDOT:PSS:Cu-Au NPs | spin coating | P3HT:PC$_{61}$BM/Ca/Al | 0.64 | 10.91 | 52.3 | 3.63 | [59] |
| | | PTB7-Th:PC$_{61}$BM/Ca/Al | 0.80 | 15.50 | 57.9 | 7.13 | |
| | | PTB7-Th:PC$_{71}$BM/Ca/Al | 0.79 | 17.78 | 60.1 | 8.48 | |
| ITO/CuS:PEDOT:PSS | spin coating | P3HT:PC$_{61}$BM/LiF/Al | 0.55 | 14.78 | 55.4 | 4.51 | [60] |
| ITO/PEDOT:PSS+ZnSTe | spin coating | P3HT:PC$_{71}$BM/Al | 0.61 | 7.51 | 44.0 | 2.03 | [61] |
| ITO/PEDOT:PSS/BPQD | spin coating | PTB7-Th:PC$_{71}$BM/PFN/Al | 0.80 | 16.40 | 69.4 | 9.11 | [62] |
| | | PM6:IT-4F/PFN/Al | 0.85 | 21.14 | 71.3 | 12.81 | |
| ITO/PEDOT:PSS+Au NPs | spin coating | P3HT:PCBM/Al | 0.61 | 9.94 | 53.3 | 3.23 | [65] |
| ITO/Au NPs/PEDOT:PSS | spin coating | P3HT:PCBM/Al | 0.66 | 9.58 | 51.1 | 3.25 | [66] |
| ITO/AuNPs/PEDOT:PSS | spin coating | P3HT:PCBM/Al | 0.59 | 7.16 | 61.0 | 3.45 | [67] |
| ITO/PEDOT:PSS-AuNRs | spin coating | PTB7-Th:PC$_{71}$BM-Au NRs/LiF/Al | 0.80 | 17.90 | 68.8 | 9.89 | [68] |
| ITO/AuQDs:PEDOT:PSS | spin coating | P3HT:PCBM/Al | 0.62 | 7.83 | 54.0 | 3.54 | [69] |
| ITO/PEDOT:PSS:(NaYF$_4$:Er$^{3+}$,Yb$^{3+}$) UC NPs:PEDOT:PSS | spin coating | P3HT:PC$_{61}$BM/Ca/Al | 0.60 | 9.44 | 53.0 | 3.02 | [71] |
| ITO/PEDOT:PSS/AgZn NPs | spin coating | P3HT:PCBM/LiF/Al | 0.55 | 14.00 | 47.0 | 3.60 | [72] |
| ITO/PEDOT:PSS+AuNRs | spin coating | PTB7:PC$_{61}$BM/E-GaIn | 0.75 | 9.43 | 67.1 | 4.50 | [73] |

| PEDOT:PSS with MO | | | | | | | |
|---|---|---|---|---|---|---|---|
| ITO/PEDOT:PSS/$V_2O_5$ | spin coating | P3HT:PCBM/Ca/Al | 0.63 | 9.34 | 64.0 | 3.75 | [75] |
| $VO_x$:PEDOT:PSS/Ag | spin coating | ITO/ZnO/TPD-3F:IT-4F | 0.87 | 16.90 | 69.4 | 10.20 | [76] |
| ITO/PEDOT:PSS-$MoO_3$ | spray deposition | PTB7:$PC_{71}BM$/Al | 0.69 | 15.20 | 48.3 | 5.11 | [77] |
| ITO/$WO_x$:PEDOT:PSS | spin coating | PM6:IT-4F/PFN-Br/Al | 0.87 | 20.73 | 80.8 | 14.57 | [78] |
| $WO_3$/PEDOT:PSS/Ag | spin coating | ITO/ZnO/SMD2:ITIC-Th | 0.90 | 17.30 | 66.0 | 10.30 | [79] |
| ITO/PEDOT:PSS/$V_2O_5$ | spin coating | P3HT:PCBM/Al | 0.66 | 9.30 | 58.0 | 3.56 | [80] |
| ITO/$V_2O_5$: PEDOT:PSS | spin coating | PTB7-Th:$PC_{71}BM$/PDINO/Al | 0.80 | 16.83 | 70.1 | 9.44 | [81] |
| PEDOT:PSS+$MoO_3$ NPs /Ag | spin coating/ blade coated | ITO/ZnO/PTB7-Th:$PC_{60}BM$ | 0.78 | 14.99 | 63.0 | 7.39 | [82] |
| ITO/PEDOT:PSS-$MoO_3$ | spin coating | PM6:IT-4F/ZnO/Ag | 0.86 | 21.71 | 70.6 | 13.19 | [83] |
| ITO/ZnO:CNT/PEDOT:PSS | spin coating | P3HT:PCBM/LiF/Al | 0.53 | 14.00 | 55.0 | 4.10 | [84] |
| AgNWs/PEDOT:PSS/$H_xMoO_3$ | transfer printing | PM6:IDIC:Y6/ZnO/AgNWs@PI | 0.83 | 21.00 | 68.0 | 11.90 | [85] |
| PMA:PEDOT:PSS/Al | spin coating | ITO/ZnO/P3HT:$PC_{61}BM$ | 0.61 | 9.17 | 64.0 | 3.44 | [86] |
| | | ITO/ZnO/PTB7-Th:$PC_{71}BM$ | 0.79 | 17.10 | 68.0 | 8.88 | |
| | | ITO/ZnO/PffBT4T-2OD:$PC_{71}BM$ | 0.77 | 18.44 | 64.0 | 8.75 | |
| PMA:PEDOT:PSS/Ag NWs | doctor-blade coating | ITO/ZnO/PTB7-Th:$PC_{71}BM$ | 0.78 | 11.28 | 57.0 | 5.01 | |
| PEDOT:PSS with GO | | | | | | | |
| ITO/GOs/PEDOT:PSS | spin coating | PBDB-T:ITIC/PFN/Al | 0.90 | 15.10 | 65.7 | 8.93 | [87] |
| Glass/GO/PEDOT:PSS | chemical vapour deposition/ drop casting | PTB7:$PC_{71}BM$/ZnO/ZnMgO/Al | 0.75 | 16.10 | 69.5 | 8.40 | [88] |
| ITO/GO/PEDOT:PSS | spin coating | P3HT:$PC_{60}BM$/PCBM/Al | 0.48 | 13.62 | 68.0 | 4.52 | [89] |
| ITO/PEDOT:PSS-GO | spin coating | P3HT:PCBM/LiF/Al | 0.53 | 14.00 | 38.0 | 2.80 | [90] |
| PEDOT:PSS/GO/Ag | spin coating | ITO/ZnO/P3HT:PCBM | 0.52 | 12.57 | 47.0 | 3.06 | [91] |
| GO/PEDOT:PSS/Au | spin coating | ITO/ZnO/P3HT:$PC_{71}BCM$ | 0.58 | 7.59 | 62.5 | 2.75 | [92] |
| ITO/PEDOT:PSS-rGO-Ge QDs | spin coated | P3HT:PCBM/LiF/Al | 0.51 | 10.30 | 46.0 | 2.40 | [93] |
| ITO/PEDOT:PSS:GO | spin coating | PTB7:PCBM/PFN/Al | 0.75 | 14.90 | 67.5 | 7.68 | [94] |
| ITO/PEDOT:PSS :GO | spin casting | PTB7:$PC_{71}BM$/Al | 0.65 | 15.17 | 53.0 | 5.22 | [97] |
| | | P3HT:$PC_{61}BM$/Al | 0.60 | 7.87 | 50.0 | 2.44 | |

| | | | | | | | |
|---|---|---|---|---|---|---|---|
| ITO/GO/PEDOT:PSS | spin coating | PCDTBT:PC$_{71}$BM/Al | 0.82 | 10.44 | 50.0 | 4.28 | [98] |
| ITO/PEDOT:PSS :GO | spin coating | P3HT:PC$_{60}$BM/ZnO/Au | 0.49 | 15.42 | 64.0 | 4.82 | [99] |
| ITO/GO/PEDOT:PSS | spin coating | PCDTBT:PC$_{71}$BM/Al | 0.85 | 10.82 | 57.0 | 5.24 | [101] |
| ITO/PEDOT:PSS-graphene | spin coating | P3HT:PCBM/Al | 0.58 | 8.30 | 52.0 | 2.50 | [102] |
| ITO/PEDOT:PSS/WS$_2$ | spun coated | P3HT:PC$_{61}$BM/Ca/Al | 0.57 | 8.39 | 64.6 | 3.07 | [103] |
| | | PTB7-Th:PC$_{71}$BM/PFN/Al | 0.79 | 15.67 | 58.6 | 7.24 | |
| ITO/PEDOT:PSS-WSe$_2$ | spin coating | PTB7:PC$_{71}$BM/Al | 0.78 | 16.60 | 65.5 | 8.50 | [104] |
| ITO/PEDOT:PSS/MoS$_2$ | spin coating | P3HT:PCBM/LiF/Al | 0.67 | 9.02 | 62.2 | 3.74 | [105] |
| ITO/PEDOT:PSS:bf-MWCNTs | spin coating | PCDTBT:PC$_{71}$BM/LiF/Al | 0.88 | 12.51 | 63.1 | 6.95 | [106] |
| ITO/g-C$_3$N$_4$:PEDOT:PSS | spin coating | PM6:Y6/PFN-Br/Ag | 0.84 | 26.71 | 73.0 | 16.38 | [107] |
| ITO/uSWNTs/PEDOT:PSS | spin coating | PM6:IT-4F/PFN-Br/Al | 0.85 | 23.39 | 73.2 | 14.60 | [108] |
| ITO/PEDOT:PSS/Ti$_3$C$_2$T$_x$ | selectively etching/ spin coating | PBDB-T:ITIC/PFN-Br/Al | 0.91 | 17.08 | 70.9 | 11.02 | [109] |
| | | PM6:Y6/PFN-Br/Al | 0.83 | 25.63 | 68.4 | 14.55 | |
| Other conjugated polymers | | | | | | | |
| ITO/PhNa-1T | spin coating | PTB7:PC$_{71}$BM/TiO$_2$/Al | 0.75 | 16.17 | 68.6 | 8.38 | [110] |
| | | PTB7-Th:PC$_{71}$BM/bis-C$_{60}$/Ag | 0.79 | 16.98 | 71.1 | 9.89 | |
| ITO/PhNa-DTBT | spin coating | PTB7-Th:PC$_{71}$BM/TiO2/Al | 0.79 | 16.92 | 69.5 | 9.29 | [111] |
| ITO/PCP-Na | spin coating | PBDT-TS1:PC$_{71}$BM/Mg/Al | 0.80 | 17.46 | 70.6 | 9.89 | [112] |
| ITO/PFSe | spin casting | PTB7:PC$_{71}$BM/PFN/Al | 0.68 | 14.40 | 69.0 | 7.20 | [113] |
| ITO/PCPDT-T | spin casting | PTB7-Th:PC$_{71}$BM/PFN/Al | 0.77 | 18.92 | 63.5 | 9.30 | [114] |
| ITO/CPE-PCPDT-K | spin coating | P3HT:PCBM/Al | 0.61 | 7.88 | 63.0 | 3.11 | [115] |
| ITO/PCPDffPhSO3K | spin coating | PTB7-Th:PC$_{71}$BM/PFN/Al | 0.79 | 18.08 | 67.0 | 9.50 | [116] |
| ITO/PFtT-D | spin coated | PTB7-Th:PC$_{71}$BM/PFN/Al | 0.76 | 16.00 | 68.4 | 8.30 | [117] |
| ITO/PCPDTKH-TT | wire-bar coating | PM6:Y6:PC$_{71}$BM/PFN/Al | 0.85 | 25.10 | 75.9 | 16.30 | [118] |
| ITO/NiOx:PFN | spin casting | PBDTTBO-C8:PC$_{71}$BM/Ca/Al | 0.71 | 13.75 | 63.7 | 6.20 | [119] |
| ITO/Cu$_2$O/FBT-TH4 | sputtered method | PffBT4T-2OD:PC$_{71}$BM/PDINO/Al | 0.77 | 17.50 | 70.7 | 9.56 | [120] |
| ITO/P3HT-Si | grafting onto, spin coating | P3HT:PC$_{61}$BM/Ca/Al | 0.49 | 10.71 | 61.0 | 3.18 | [122] |
| FTO/PEDOT:PSS/P3HT:SWCNTs | spin coated | P3HT:PCBM/Al | 0.55 | 8.48 | 54.0 | 2.52 | [123] |

| | | | | | | |
|---|---|---|---|---|---|---|
| ITO/Au-Ag-PANI | spin coating | P3HT:PCBM/Al | 0.48 | 8.50 | 61.0 | 2.44 | [124] |
| ITO/CNT-g-PDDT:P3ThEt-g-PANI | spin coating | PBDT-DTNT:PC$_{61}$BM/LiF/Al | 0.71 | 12.84 | 62.0 | 5.65 | [125] |
| | | PBDT-TIPS-DTNT-DT:PC$_{61}$BM/LiF/Al | 0.69 | 11.59 | 60.0 | 4.80 | |
| ITO/CNt:P3ThEt-g-PANI | spin coating | P3HT:PC$_{71}$BM/LiF/Al | 0.68 | 12.85 | 60.7 | 5.30 | [126] |
| ITO/PANI:PSS | spin coating | P3HT:ICBA/Ca/Al | 0.84 | 8.50 | 62.4 | 4.50 | [127] |
| ITO/CuSCN/TFB | spin coating | PM6:Y6/BCP/Al | 0.85 | 24.45 | 72.7 | 15.10 | [131] |
| | | PTB7-Th:PC$_{71}$BM/PFN/Al | 0.79 | 16.42 | 66.3 | 8.56 | |

## 2.2 Small organic molecules

As an alternative to conjugated polymers, small organic molecules can be used as HTLs for photovoltaic applications [20]. The molecular structure of small molecules used as HTL are shown in Figure 14. For instance, (NDP9) doped N,N'-((diphenyl-N,N'-bis)9,9,-dimethyl-fluoren-2-yl)-benzidine (BF-DPB) was used as hole transport material in OSC based on zinc phtalocyanine (ZnPC):fullerene $C_{60}$ [132]. Spin-coated BF-DPB HTLs over AgNWs electrodes exhibited a PCE of 4.4%. BF-DPB smoothed AgNWs topography. However, the $V_{oc}$ was low, explained by an unfavorable direct contact of p-doped HTL and the BHJ. *Cheng et al.* fabricated NiOx / 2,3,5,6-tetrafluoro-7,7,8,8-tetracyanoquinodimethane (F4-TCNQ) composite HTLs, for the fabrication of OSCs without pre-treatment of ITO nor post-treatment on the HTL [133]. The device performance (PCE of 3.59%) of one-step ethanol processed NiOx:F4-TCNQ in P3HT:$PC_{61}$BM based OSCs was 15.8% better than one-step PEDOT:PSS based OSCs. NiOx:F4-TCNQ HTL was also used on PTB7-Th:$PC_{71}$BM based OSCs resulting in an enhanced PCE of 8.59% (see Figure 12 (b)).
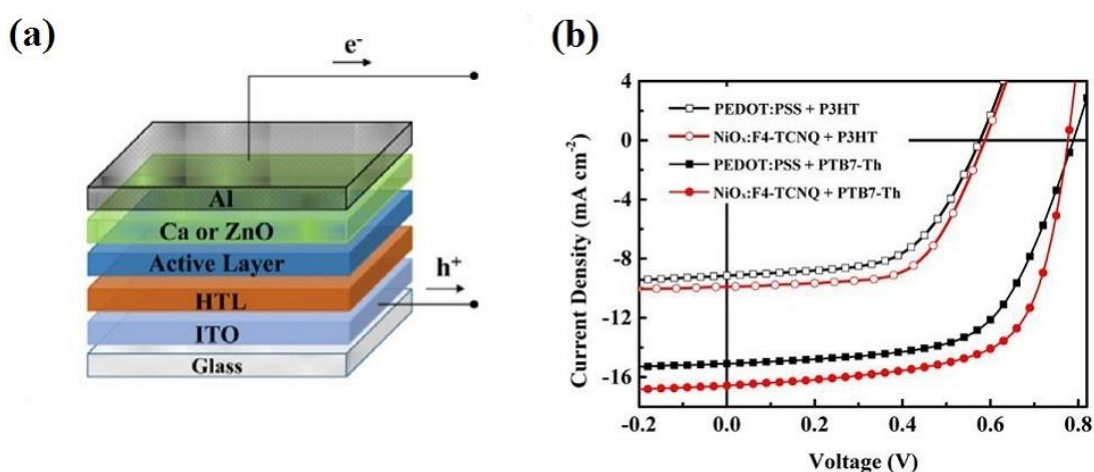


Figure 12. (a) Device structure of OSC, and (b) J-V characteristics under AM 1.5 G solar spectrum of OSCs with a structure of ITO/HTL(PEDOT:PSS or NiOx:F4-TCNQ )/Active layer/Ca/Al [133].

A planar quinoid molecule, 2,2',6,6'-tetraphenyl-dipyranylidene (DIPO-Ph4) was tested as an anodic interfacial layer with PEDOT:PSS in P3HT:PCBM OSCs [134]. Vacuum deposited DIPO-Ph4 (10 nm thickness) / spin-coated PEDOT:PSS (5 nm thickness) HTL increased OSCs' current and enhanced efficiency to 4.6%. DIPO-Ph4 needle-like morphology increased the contact area between the active layer and the anode with high hole conductivity. 1,3,4,5,6,7-

Hexaphenyl-2-{3'-(9-ethylcarbazolyl)}-isoindole (HPCzI) HTLs exhibited improved performance in comparison to $MoO_3$ based OSCs, reaching a PCE of 1.69% for CuPC:C60 based OSCs, due to larger FF and $J_{sc}$ [135]. An additional improvement (PCE of 1.71%) was observed when $MoO_3$ doped HPCzI was used as HTL due to higher hole mobility. N, N′-bis(1-naphthalenyl)N,N′-bis-phenyl-(1, 1′-biphenyl)-4, 4′-diamine (NPB) was incorporated as HTL on inverted P3HT:PC$_{71}$BM OSCs resulting in a PCE of 2.63%, a $J_{sc}$ of 9.49 mA cm$^{-2}$ and low $R_s$ [136]. These results suggested the formation of ohmic contact between the photoactive layer and anode, which contributed to the hole extraction efficiency. Alternatively, NPB layer was inserted between $MoO_3$ layer and the photoactive layer in an inverted OSCs based on P3HT:PC$_{61}$BM [137]. The PCE was enhanced from 3.20% to 3.94%, owing to the increased $J_{sc}$ and reduced $R_s$ by an improved charge transportation and reduced recombination at the interface. $MoO_3$ p-doped 4,4′-N,N′-dicarbazole-biphenyl (CBP:$MoO_3$) was also utilized as HTLs in inverted P3HT:PC$_{61}$BM based OSCs [138]. 3,6,11,14-Tetramethoxyphenylamine-dibenzo[g,p]chrysene (MeOPhN-DBC) layer was incorporated between $MoO_3$ and active layer P3HT:PC$_{61}$BM inverted OSCs showing an enhanced PCE of 3.68%, attributed to improved $J_{sc}$ and FF, and small leakage current [139]. Liu *et al.* reported a tetrathiafulvalene derivative with four carboxyl groups (TTA) as an HTL in OSCs [140]. This HTL displayed a well-matched energy level (Figure 13 (b)) and an enhanced PCE of 9.09% in comparison to a PEDOT:PSS based OSC (see Figure 13(c)). The improved FF and $J_{SC}$ were related to the smooth surface of the TTA layer, improved charge transfer and hole mobility, and reduced charge recombination. Finally, Table 2 summarizes the device parameters of some OSCs with small organic molecules used as HTLs.
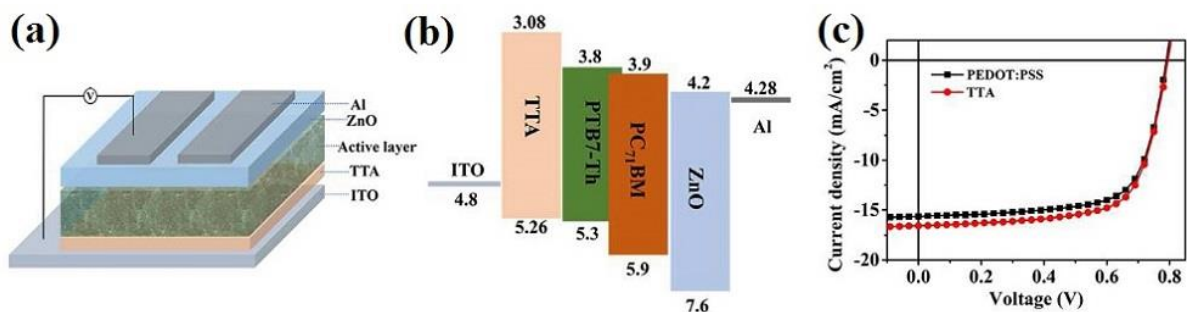


Figure 13. (a) Illustration of OSCs structure based on TTA, (b) energy level diagram of different layers, and (c) J-V curves of devices with TTA and PEDOT:PSS as HTLs [140].
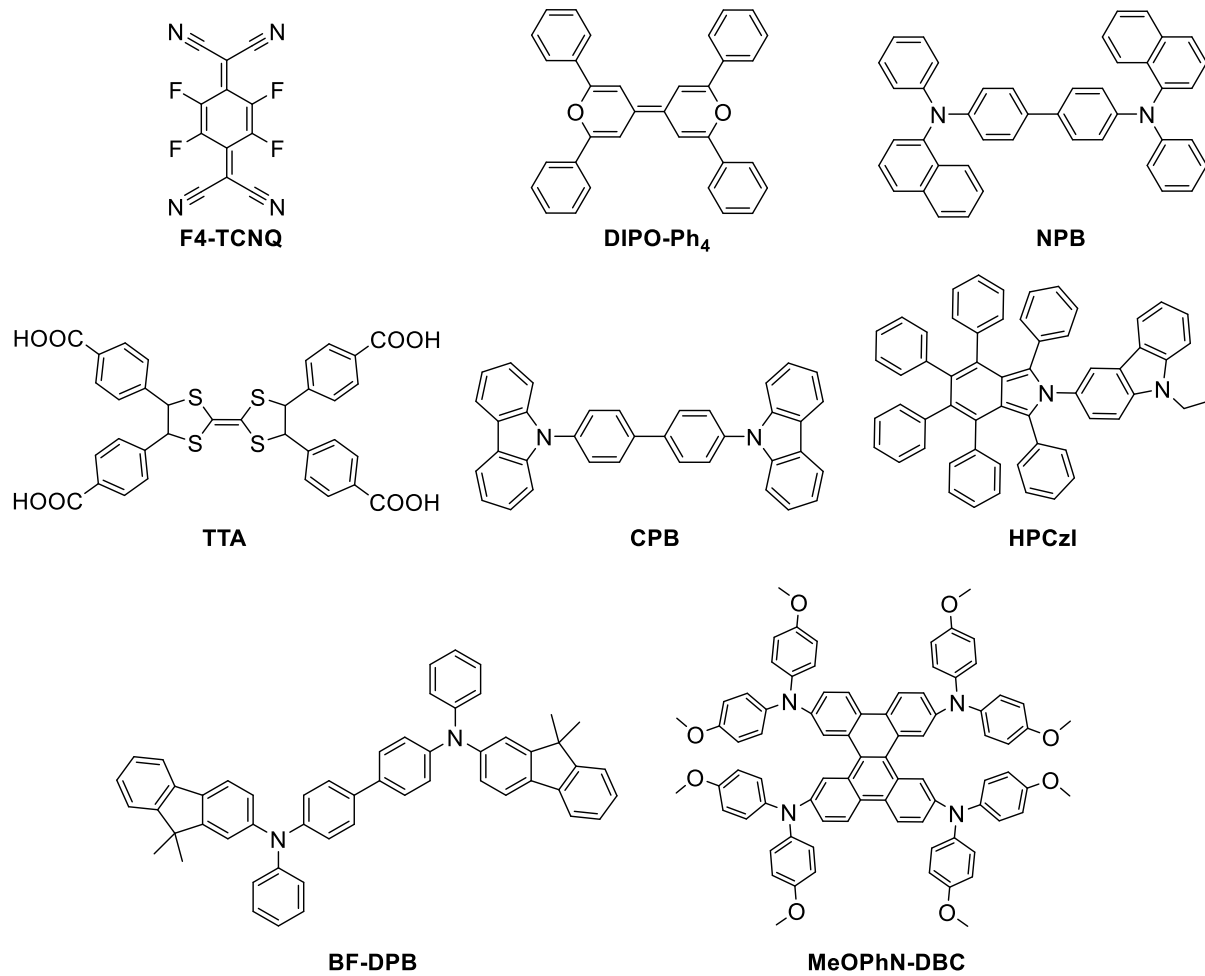
Figure 14. Molecular structure of some small organic molecules used for HTL.

Table 2. Device characteristics of some representative OSCs with different small organic molecules as HTLs

| Anode configuration | Deposition technique | Remaining architecture cell | $V_{OC}$ (V) | $J_{SC}$ (mA cm$^{-2}$) | FF (%) | PCE (%) | Ref. |
|---|---|---|---|---|---|---|---|
| ITO/BF-DPB:NDP9 | spin coating | ZnPC:$C_{60}$/Al | 0.51 | 7.50 | 55.00 | 2.10 | [132] |
| Ag NWs/BF-DPB:NDP9 | | ZnPC:$C_{60}$/Al | 0.49 | 7.60 | 55.00 | 2.10 | |
| ITO/NiO$_x$:F4-TCNQ | spin coating | P3HT:$PC_{61}BM$/Ca/Al | 0.59 | 9.89 | 61.60 | 3.59 | [133] |
| | | PTB7-Th:$PC_{71}BM$/Ca/Al | 0.78 | 16.80 | 65.20 | 8.59 | |
| ITO/DIPO-Ph$_4$/PEDOT:PSS | vacuum deposition/ spin coating | P3HT:$PC_{61}BM$/LiF/Al | 0.60 | 11.50 | 47.00 | 4.60 | [134] |
| NPB/Ag | vacuum deposition | ITO/ZnO/P3HT:$PC_{71}BM$ | 0.57 | 9.49 | 48.90 | 2.63 | [136] |
| NPB/MoO$_3$/Ag | thermal evaporation | ITO/PEIE/P3HT:$PC_{61}BM$ | 0.60 | 10.04 | 63.00 | 3.94 | [137] |
| ITO/TTA | spin coating | PTB7-Th:$PC_{71}BM$/ZnO/Al | 0.80 | 16.56 | 69.04 | 9.09 | [140] |
| ITO/HPCzI | thermal evaporation | CuPC:$C_{60}$/$C_{60}$/TPBi/Al | 0.49 | 6.22 | 53.00 | 1.62 | [135] |
| ITO/MoO$_3$:HPCzI | | CuPC:$C_{60}$/$C_{60}$/TPBi/Al | 0.49 | 6.63 | 53.00 | 1.71 | |
| MeOPhN-DBC/MoO$_3$/Al | vacuum deposition | FTO/TiO$_2$/P3HT:$PC_{61}BM$ | 0.63 | 12.44 | 47.00 | 3.68 | [139] |

# 3 CONCLUSIONS AND RECOMMENDATIONS

## 3.1 CONCLUSIONS

This literature review of conducting polymer used as HTLs showed that the most used conjugated polymer is the PEDOT:PSS and their composites such as PEDOT:PSS with NPs, with MOs and with GO either in bilayer or composite monolayer. PANI was the second choice of conducting polymers as HTLs. The different modification to PEDOT:PSS in many cases increases the $J_{SC,}$ improves the conductivity, and decreases the recombination loss of the device. In general, the addition of metallic NPs to PEDOT:PSS enhances the absorption ability of the photoactive layer, increases the conductivity, and improves the charge carrier collection by increasing the device performance. The incorporation of metal oxides mainly helps to (i) increase the stability of the device (e.g., $MoO_3$) by mitigating the degradation, (ii) serves as an electron blocking layer (e.g., $V_2O_5$), and (iii) suppress the charge recombination. On the other hand, GO addition to PEDOT:PSS improves the conductivity and increases the device resistance to degradation. Furthermore, CPEs were also used as HTL for OSCs; in general, these materials, were pH neutral layers that improved the stability of the devices and showed high electrical conductivity and good interface compatibility. Small organic molecules had also been used as HTLs with less prominence.

## 3.2 RECOMMENDATIONS

As it has been shown PEDOT:PSS has some limitations in terms of device stability, so the replacement of PSS is recommended as a good alternative since PSS provides a strong acidic nature that causes the degradation.

Also, conjugated polymer composites with NP, MO, and GO are recommended instead of only PEDOT:PSS. These conjugated polymer composites enhance the conductivity and improve other parameters of the photovoltaic device. Composites of PEDOT:PSS and metallic NP are recommended when needed to enhance the current through the increase of of the photoactive layer's absorption capability. Composites of PEDOT:PSS and MO are recommended because they tend to increase the device's stability and function as effective electron blocking materials. Composites of PEDOT:PSS and GO are recommended to increases the conductivity and stability of the device.

To avoid the acidic nature of PEDOT:PSS is also recommended to use conjugated polyelectrolytes as HTLs. CPEs are neutral, conductive, and present good compatibility with the other layers.

Also, it is recommended that research around HTL focus on processability, stability, and efficiency of the photovoltaic device and not just in one of these areas. So, it is important that research of conducting polymers as HTLs focuses on contributing to OSCs' stability; this can be achieved by the use of PEDOT:PSS composites with MO and CPE.

Furthermore, it is recommended that the deposition technique of layers be compatible with roll-to-roll processing to ensure that it can be large-area manufactured, making OSCs more competitive, as slot-die coating and knife-over-edge coating and printing techniques.

# REFERENCES

[1] IEA, "Global Energy Review 2019," 2020. https://www.iea.org/reports/global-energy-review-2019.

[2] S. B. Darling and F. You, "The case for organic photovoltaics," *RSC Adv.*, vol. 3, no. 39, pp. 17633–17648, 2013, doi: 10.1039/c3ra42989j.

[3] B. Looney, "Statistical Review of World Energy, 2020 | 69th Edition," *Bp*, vol. 69, 2020.

[4] Worldometers.info, "World Population Clock: 7.8 Billion People (2021)," *Current World Population*, 2021. https://www.worldometers.info/world-population/.

[5] Hannah Ritchie, "Energy," *Our World Data*, 2014, [Online]. Available: https://ourworldindata.org/energy.

[6] W. Hermes, D. Waldmann, M. Agari, K. Schierle-Arndt, and P. Erk, "Emerging thin-film photovoltaic technologies," *Chemie-Ingenieur-Technik*, vol. 87, no. 4. 2015, doi: 10.1002/cite.201400101.

[7] M. Jacoby, *The future of low-cost solar cells*, vol. 94. 2016.

[8] M. Riede, D. Spoltore, and K. Leo, "Organic Solar Cells—The Path to Commercial Success," *Adv. Energy Mater.*, vol. 11, no. 1, p. 2002653, Jan. 2021, doi: 10.1002/aenm.202002653.

[9] F. C. Krebs, N. Espinosa, M. Hösel, R. R. Søndergaard, and M. Jørgensen, "25th anniversary article: Rise to power - OPV-based solar parks," *Adv. Mater.*, vol. 26, no. 1, pp. 29–39, 2014, doi: 10.1002/adma.201302031.

[10] Q. Liu *et al.*, "18% Efficiency organic solar cells," *Sci. Bull.*, vol. 65, no. 4, pp. 272–275, Feb. 2020, doi: 10.1016/j.scib.2020.01.001.

[11] M. Green, E. Dunlop, J. Hohl-Ebinger, M. Yoshita, N. Kopidakis, and X. Hao, "Solar cell efficiency tables (version 57)," *Prog. Photovoltaics Res. Appl.*, vol. 29, no. 1, pp. 3–15, Jan. 2021, doi: 10.1002/pip.3371.

[12] M. B. Salim, R. Nekovei, and R. Jeyakumar, "Organic tandem solar cells with 18.6% efficiency," *Sol. Energy*, vol. 198, pp. 160–166, Mar. 2020, doi: 10.1016/j.solener.2020.01.042.

[13] C. Yan *et al.*, "Non-fullerene acceptors for organic solar cells," *Nature Reviews Materials*, vol. 3. 2018, doi: 10.1038/natrevmats.2018.3.

[14] C. Duan, F. Huang, and Y. Cao, "Solution processed thick film organic solar cells," *Polym. Chem.*, vol. 6, no. 47, pp. 8081–8098, 2015, doi: 10.1039/c5py01340b.

[15] M. C. Scharber and N. S. Sariciftci, "Efficiency of bulk-heterojunction organic solar cells," *Prog. Polym. Sci.*, vol. 38, no. 12, pp. 1929–1940, Dec. 2013, doi: 10.1016/j.progpolymsci.2013.05.001.

[16] N. Yeh and P. Yeh, "Organic solar cells: Their developments and potentials," *Renew. Sustain. Energy Rev.*, vol. 21, pp. 421–431, May 2013, doi: 10.1016/j.rser.2012.12.046.

[17] A. J. Heeger, "25th Anniversary Article: Bulk Heterojunction Solar Cells: Understanding the Mechanism of Operation," *Adv. Mater.*, vol. 26, no. 1, pp. 10–28, Jan. 2014, doi: 10.1002/adma.201304373.

[18] K. A. Mazzio and C. K. Luscombe, "The future of organic photovoltaics," *Chem. Soc. Rev.*, vol. 44, no. 1, pp. 78–90, 2015, doi: 10.1039/C4CS00227J.

[19] Z. Hu *et al.*, "A critical review on semitransparent organic solar cells," *Nano Energy*, vol. 78, p. 105376, Dec. 2020, doi: 10.1016/j.nanoen.2020.105376.

[20] J. H. Park, T.-W. Lee, B.-D. Chin, D. H. Wang, and O. O. Park, "Roles of Interlayers in Efficient Organic Photovoltaic Devices," *Macromol. Rapid Commun.*, vol. 31, no. 24, pp. 2095–2108, Dec. 2010, doi: 10.1002/marc.201000310.

[21] T.-H. Lai, S.-W. Tsang, J. R. Manders, S. Chen, and F. So, "Properties of interlayer for organic photovoltaics," *Mater. Today*, vol. 16, no. 11, pp. 424–432, Nov. 2013, doi: 10.1016/j.mattod.2013.10.001.

[22] R. Steim, F. R. Kogler, and C. J. Brabec, "Interface materials for organic solar cells," *J. Mater. Chem.*, vol. 20, no. 13, p. 2499, 2010, doi: 10.1039/b921624c.

[23] R. Po, C. Carbonera, A. Bernardi, and N. Camaioni, "The role of buffer layers in polymer solar cells," *Energy Environ. Sci.*, vol. 4, no. 2, pp. 285–310, 2011, doi: 10.1039/C0EE00273A.

[24] L. S. Roman, W. Mammo, L. A. A. Pettersson, M. R. Andersson, and O. Inganäs, "High Quantum Efficiency Polythiophene," *Adv. Mater.*, vol. 10, no. 10, pp. 774–777, Jul.

1998, doi: 10.1002/(SICI)1521-4095(199807)10:10<774::AID-ADMA774>3.0.CO;2-J.

[25]  R. Po, C. Carbonera, A. Bernardi, and N. Camaioni, "The role of buffer layers in polymer solar cells," *Energy Environ. Sci.*, vol. 4, no. 2, pp. 285–310, 2011, doi: 10.1039/c0ee00273a.

[26]  S. B. Darling and F. You, "The case for organic photovoltaics," *RSC Adv.*, vol. 3, no. 39, p. 17633, 2013, doi: 10.1039/c3ra42989j.

[27]  J. G. Ibanez, M. E. Rincón, S. Gutierrez-Granados, M. Chahma, O. A. Jaramillo-Quintero, and B. A. Frontana-Uribe, "Conducting Polymers in the Fields of Energy, Environmental Remediation, and Chemical-Chiral Sensors," *Chem. Rev.*, vol. 118, no. 9, pp. 4731–4816, 2018, doi: 10.1021/acs.chemrev.7b00482.

[28]  J. B. Emah, N. J. George, and U. B. Akpan, "Interfacial Surface Modification via Nanoimprinting to Increase Open-Circuit Voltage of Organic Solar Cells," *J. Electron. Mater.*, vol. 46, no. 8, pp. 4989–4998, 2017, doi: 10.1007/s11664-017-5472-2.

[29]  M. Fernández Castro, E. Mazzolini, R. R. Sondergaard, M. Espindola-Rodriguez, and J. W. Andreasen, "Flexible ITO-Free Roll-Processed Large-Area Nonfullerene Organic Solar Cells Based on P3HT:O-IDTBR," *Phys. Rev. Appl.*, vol. 14, no. 3, p. 34067, Sep. 2020, doi: 10.1103/PhysRevApplied.14.034067.

[30]  V. Vohra, S. Shimizu, and Y. Takeoka, "Water-Processed Organic Solar Cells with Open-Circuit Voltages Exceeding 1.3V," *Coatings*, vol. 10, no. 4, p. 421, Apr. 2020, doi: 10.3390/coatings10040421.

[31]  T. M. Abdel-Fattah, E. M. Younes, G. Namkoong, E. M. El-Maghraby, A. H. Elsayed, and A. H. Abo Elazm, "Solvents effects on the hole transport layer in organic solar cells performance," *Sol. Energy*, vol. 137, pp. 337–343, Nov. 2016, doi: 10.1016/j.solener.2016.08.023.

[32]  M. Yi *et al.*, "Modification of a PEDOT:PSS hole transport layer for printed polymer solar cells," *Sol. Energy Mater. Sol. Cells*, vol. 153, pp. 117–123, Aug. 2016, doi: 10.1016/j.solmat.2016.04.023.

[33]  H. Tang, Z. Liu, Z. Hu, Y. Liang, F. Huang, and Y. Cao, "Oxoammonium enabled secondary doping of hole transporting material PEDOT:PSS for high-performance

organic solar cells," *Sci. China Chem.*, vol. 63, no. 6, pp. 802–809, Jun. 2020, doi: 10.1007/s11426-020-9729-y.

[34]  C. T. Howells *et al.*, "Enhanced organic solar cells efficiency through electronic and electro-optic effects resulting from charge transfers in polymer hole transport blends," *J. Mater. Chem. A*, vol. 4, no. 11, pp. 4252–4263, 2016, doi: 10.1039/c6ta00677a.

[35]  N. Hong *et al.*, "Unexpected fluorescent emission of graft sulfonated-acetone-formaldehyde lignin and its application as a dopant of PEDOT for high performance photovoltaic and light-emitting devices," *J. Mater. Chem. C*, vol. 4, no. 23, pp. 5297–5306, 2016, doi: 10.1039/c6tc01170e.

[36]  W. Cai *et al.*, "Self-doped conjugated polyelectrolyte with tuneable work function for effective hole transport in polymer solar cells," *J. Mater. Chem. A*, vol. 4, no. 40, pp. 15670–15675, 2016, doi: 10.1039/C6TA04989C.

[37]  Ç. K. Kurukavak and S. Polat, "Influence of the volume of EGME-DMSO mixed co-solvent doping on the characteristics of PEDOT:PSS and their application in polymer solar cells," *Polym. Polym. Compos.*, p. 96739112096347, Oct. 2020, doi: 10.1177/0967391120963470.

[38]  R. Bhargav, D. Bhardwaj, Shahjad, A. Patra, and S. Chand, "Poly(Styrene Sulfonate) Free Poly(3,4-Ethylenedioxythiophene) as a Robust and Solution-Processable Hole Transport Layer for Organic Solar Cells," *ChemistrySelect*, vol. 1, no. 7, pp. 1347–1352, May 2016, doi: 10.1002/slct.201600202.

[39]  O. L. Gribkova *et al.*, "Ultraviolet-Visible-Near Infrared and Raman spectroelectrochemistry of poly(3,4-ethylenedioxythiophene) complexes with sulfonated polyelectrolytes. The role of inter- and intra-molecular interactions in polyelectrolyte," *Electrochim. Acta*, vol. 222, pp. 409–420, Dec. 2016, doi: 10.1016/j.electacta.2016.10.193.

[40]  D. H. Kim, D. J. Lee, B. Kim, C. Yun, and M. H. Kang, "Tailoring PEDOT:PSS polymer electrode for solution-processed inverted organic solar cells," *Solid. State. Electron.*, vol. 169, p. 107808, Jul. 2020, doi: 10.1016/j.sse.2020.107808.

[41]  L. Liu *et al.*, "Performance Enhancement of Conventional Polymer Solar Cells with TTF-py-Modified PEDOT:PSS Film as the Hole Transport Layer," *ACS Appl. Energy*

*Mater.*, vol. 2, no. 9, pp. 6577–6583, Sep. 2019, doi: 10.1021/acsaem.9b01125.

[42]    J. Wang *et al.*, "Regulating Bulk-Heterojunction Molecular Orientations through Surface Free Energy Control of Hole-Transporting Layers for High-Performance Organic Solar Cells," *Adv. Mater.*, vol. 31, no. 17, p. 1806921, Apr. 2019, doi: 10.1002/adma.201806921.

[43]    M. A. Khan and U. Farva, "Elucidation of hierarchical metallophthalocyanine buffer layers in bulk heterojunction solar cells," *RSC Adv.*, vol. 7, no. 19, pp. 11304–11311, 2017, doi: 10.1039/C6RA26919B.

[44]    J. Wang, H. Yu, C. Hou, and J. Zhang, "Solution-Processable PEDOT:PSS:α-In 2 Se 3 with Enhanced Conductivity as a Hole Transport Layer for High-Performance Polymer Solar Cells," *ACS Appl. Mater. Interfaces*, vol. 12, no. 23, pp. 26543–26554, Jun. 2020, doi: 10.1021/acsami.0c02489.

[45]    M. Zeng *et al.*, "Dopamine Semiquinone Radical Doped PEDOT:PSS: Enhanced Conductivity, Work Function and Performance in Organic Solar Cells," *Adv. Energy Mater.*, vol. 10, no. 25, p. 2000743, Jul. 2020, doi: 10.1002/aenm.202000743.

[46]    S. H. Roh and J. K. Kim, "Hexagonal Array Patterned PMMA Buffer Layer for Efficient Hole Transport and Tailored Interfacial Properties of FTO-Based Organic Solar Cells," *Macromol. Res.*, vol. 26, no. 12, pp. 1173–1178, Dec. 2018, doi: 10.1007/s13233-018-6152-7.

[47]    C. K. Kwak *et al.*, "Improved efficiency in organic solar cells via conjugated polyelectrolyte additive in the hole transporting layer," *J. Mater. Chem. C*, vol. 4, no. 45, pp. 10722–10730, 2016, doi: 10.1039/C6TC03771B.

[48]    C. Liu, H. Luo, G. Shi, L. Nian, Z. Chi, and Y. Ma, "Electrochemical route to fabricate porous organic polymers film and its application for polymer solar cells," *Dye. Pigment.*, vol. 142, pp. 132–138, Jul. 2017, doi: 10.1016/j.dyepig.2017.03.017.

[49]    Y. Li *et al.*, "Built-in voltage enhanced by in situ electrochemical polymerized undoped conjugated hole-transporting modifiers in organic solar cells," *J. Mater. Chem. C*, vol. 8, no. 8, pp. 2676–2681, 2020, doi: 10.1039/C9TC06140A.

[50]    E. J. Lee, J. P. Han, S. E. Jung, M. H. Choi, and D. K. Moon, "Improvement in Half-Life of Organic Solar Cells by Using a Blended Hole Extraction Layer Consisting of

PEDOT:PSS and Conjugated Polymer Electrolyte," *ACS Appl. Mater. Interfaces*, vol. 8, no. 46, pp. 31791–31798, Nov. 2016, doi: 10.1021/acsami.6b09846.

[51] G. E. Pérez *et al.*, "Improved Performance and Stability of Organic Solar Cells by the Incorporation of a Block Copolymer Interfacial Layer," *Adv. Mater. Interfaces*, vol. 7, no. 18, p. 2000918, Sep. 2020, doi: 10.1002/admi.202000918.

[52] M. S. G. Hamed, S. O. Oseni, A. Kumar, G. Sharma, and G. T. Mola, "Nickel sulphide nano-composite assisted hole transport in thin film polymer solar cells," *Sol. Energy*, vol. 195, pp. 310–317, Jan. 2020, doi: 10.1016/j.solener.2019.11.068.

[53] Y. Wei, Q. Zhang, H. Wan, Y. Zhang, S. Zheng, and Y. Zhang, "A facile synthesis of segmented silver nanowires and enhancement of the performance of polymer solar cells," *Phys. Chem. Chem. Phys.*, vol. 20, no. 27, pp. 18837–18843, 2018, doi: 10.1039/C8CP02734J.

[54] M. Michalska *et al.*, "Analysis of the surface decoration of TiO 2 grains using silver nanoparticles obtained by ultrasonochemical synthesis towards organic photovoltaics," *New J. Chem.*, vol. 42, no. 9, pp. 7340–7354, 2018, doi: 10.1039/C7NJ05180H.

[55] J. Hao *et al.*, "Broadband plasmon-enhanced polymer solar cells with power conversion efficiency of 9.26% using mixed Au nanoparticles," *Opt. Commun.*, vol. 362, pp. 50–58, Mar. 2016, doi: 10.1016/j.optcom.2015.07.032.

[56] Y. Oh *et al.*, "Plasmonic Periodic Nanodot Arrays via Laser Interference Lithography for Organic Photovoltaic Cells with >10% Efficiency," *ACS Nano*, vol. 10, no. 11, pp. 10143–10151, Nov. 2016, doi: 10.1021/acsnano.6b05313.

[57] A. Singh, A. Dey, D. Das, and P. K. Iyer, "Combined influence of plasmonic metal nanoparticles and dual cathode buffer layers for highly efficient rrP3HT:PCBM-based bulk heterojunction solar cells," *J. Mater. Chem. C*, vol. 5, no. 26, pp. 6578–6587, 2017, doi: 10.1039/C7TC01621B.

[58] P.-T. Sah, W.-C. Chang, J.-H. Chen, H.-H. Wang, and L.-H. Chan, "Bimetallic Ag–Au–Ag nanorods used to enhance efficiency of polymer solar cells," *Electrochim. Acta*, vol. 259, pp. 293–302, Jan. 2018, doi: 10.1016/j.electacta.2017.10.187.

[59] M. Tang *et al.*, "Broad-band plasmonic Cu-Au bimetallic nanoparticles for organic bulk heterojunction solar cells," *Org. Electron.*, vol. 38, pp. 213–221, Nov. 2016, doi:

10.1016/j.orgel.2016.08.023.

[60] M. A. Adedeji, M. S. G. Hamed, and G. T. Mola, "Light trapping using copper decorated nano-composite in the hole transport layer of organic solar cell," *Sol. Energy*, vol. 203, pp. 83–90, Jun. 2020, doi: 10.1016/j.solener.2020.04.005.

[61] M. A. Najeeb *et al.*, "A comparative study on the performance of hybrid solar cells containing ZnSTe QDs in hole transporting layer and photoactive layer," *J. Nanoparticle Res.*, vol. 18, no. 12, p. 384, Dec. 2016, doi: 10.1007/s11051-016-3694-5.

[62] X. Zhang, Q. Jiang, J. Wang, and J. Tang, "Black phosphorous quantum dots as an effective interlayer modifier in polymer solar cells," *Sol. Energy*, vol. 206, pp. 670–676, Aug. 2020, doi: 10.1016/j.solener.2020.06.007.

[63] Y. A. M. Ismail, N. Kishi, and T. Soga, "Improvement of organic solar cells using aluminium microstructures prepared in PEDOT:PSS buffer layer by using ultrasonic ablation technique," *Thin Solid Films*, vol. 616, pp. 73–79, Oct. 2016, doi: 10.1016/j.tsf.2016.08.001.

[64] A. V. Kesavan, A. K. Jagdish, and P. C. Ramamurthy, "Organic Inorganic Hybrid Hole Transport Layer for Light Management in Inverted Organic Photovoltaic," *IEEE J. Photovoltaics*, vol. 7, no. 3, pp. 787–791, 2017, doi: 10.1109/JPHOTOV.2017.2676770.

[65] F. Otieno *et al.*, "Improved efficiency of organic solar cells using Au NPs incorporated into PEDOT:PSS buffer layer," *AIP Adv.*, vol. 7, no. 8, p. 85302, Aug. 2017, doi: 10.1063/1.4995803.

[66] H. Gao, J. Meng, J. Sun, and J. Deng, "Enhanced performance of polymer solar cells based on P3HT:PCBM via incorporating Au nanoparticles prepared by the micellar method," *J. Mater. Sci. Mater. Electron.*, vol. 31, no. 13, pp. 10760–10767, Jul. 2020, doi: 10.1007/s10854-020-03626-x.

[67] S. Phetsang *et al.*, "Enhancement of organic thin-film solar cells by incorporating hybrid Au nanospheres and Au nanorods on a metallic grating surface," *Mol. Cryst. Liq. Cryst.*, vol. 705, no. 1, pp. 41–47, Jul. 2020, doi: 10.1080/15421406.2020.1741822.

[68] Z. Liu, J. Park, B. Li, H. P. Chan, D. K. Yi, and E.-C. Lee, "Performance improvement of organic bulk-heterojunction solar cells using complementary plasmonic gold nanorods," *Org. Electron.*, vol. 84, p. 105802, Sep. 2020, doi:

10.1016/j.orgel.2020.105802.

[69]  S. Phetsang *et al.*, "Enhancement of organic solar cell performance by incorporating gold quantum dots (AuQDs) on a plasmonic grating," *Nanoscale Adv.*, vol. 2, no. 7, pp. 2950–2957, 2020, doi: 10.1039/D0NA00169D.

[70]  M. Haase and H. Schäfer, "Upconverting Nanoparticles," *Angew. Chemie Int. Ed.*, vol. 50, no. 26, pp. 5808–5829, Jun. 2011, doi: 10.1002/anie.201005159.

[71]  Y. Mei *et al.*, "Application of $\beta$-NaYF$_4$:Er$^{3+}$ (2%), Yb$^{3+}$ (18%) Up-Conversion Nanoparticles in Polymer Solar Cells and its Working Mechanism," *J. Nanosci. Nanotechnol.*, vol. 16, no. 7, pp. 7380–7387, Jul. 2016, doi: 10.1166/jnn.2016.11622.

[72]  G. T. Mola and E. A. A. Arbab, "Bimetallic nanocomposite as hole transport co-buffer layer in organic solar cell," *Appl. Phys. A*, vol. 123, no. 12, p. 772, Dec. 2017, doi: 10.1007/s00339-017-1383-6.

[73]  N. T. N. Truong, C. D. Kim, V. R. Minnam Reddy, V. H. Thai, H. J. Jeon, and C. Park, "Shape control of plasmonic gold nanoparticles and its application to vacuum-free bulk hetero-junction solar cells," *J. Mater. Sci. Mater. Electron.*, vol. 31, no. 24, pp. 22957–22965, Dec. 2020, doi: 10.1007/s10854-020-04822-5.

[74]  S. Rafique, S. M. Abdullah, W. E. Mahmoud, A. A. Al-Ghamdi, and K. Sulaiman, "Stability enhancement in organic solar cells by incorporating V 2 O 5 nanoparticles in the hole transport layer," *RSC Adv.*, vol. 6, no. 55, pp. 50043–50052, 2016, doi: 10.1039/C6RA07210K.

[75]  H. Ling, R. Zhang, X. Ye, Z. Wen, J. Xia, and X. Lu, "In-situ synthesis of organic-inorganic hybrid thin film of PEDOT/V2O5 as hole transport layer for polymer solar cells," *Sol. Energy*, vol. 190, pp. 63–68, Sep. 2019, doi: 10.1016/j.solener.2019.07.095.

[76]  N.-W. Teng *et al.*, "Highly Efficient Nonfullerene Organic Photovoltaic Devices with 10% Power Conversion Efficiency Enabled by a Fine-Tuned and Solution-Processed Hole-Transporting Layer," *Sol. RRL*, vol. 4, no. 9, p. 2000223, Sep. 2020, doi: 10.1002/solr.202000223.

[77]  T. Mohammad, C. Dwivedi, V. Kumar, and V. Dutta, "Role of Continuous Spray Pyrolyzed synthesized MoO3 nanorods in PEDOT:PSS matrix by electric field assisted

spray deposition for organic photovoltaics," *Org. Electron.*, vol. 77, p. 105525, Feb. 2020, doi: 10.1016/j.orgel.2019.105525.

[78]   Z. Zheng *et al.*, "A Highly Efficient Non-Fullerene Organic Solar Cell with a Fill Factor over 0.80 Enabled by a Fine-Tuned Hole-Transporting Layer," *Adv. Mater.*, vol. 30, no. 34, p. 1801801, Aug. 2018, doi: 10.1002/adma.201801801.

[79]   Y. W. Han *et al.*, "Evaporation-Free Nonfullerene Flexible Organic Solar Cell Modules Manufactured by An All-Solution Process," *Adv. Energy Mater.*, vol. 9, no. 42, p. 1902065, Nov. 2019, doi: 10.1002/aenm.201902065.

[80]   J. Pan, P. Li, L. Cai, Y. Hu, and Y. Zhang, "All-solution processed double-decked PEDOT:PSS/V2O5 nanowires as buffer layer of high performance polymer photovoltaic cells," *Sol. Energy Mater. Sol. Cells*, vol. 144, pp. 616–622, Jan. 2016, doi: 10.1016/j.solmat.2015.09.061.

[81]   J. Li *et al.*, "Enhanced organic photovoltaic performance through promoting crystallinity of photoactive layer and conductivity of hole-transporting layer by V2O5 doped PEDOT:PSS hole-transporting layers," *Sol. Energy*, vol. 211, pp. 1102–1109, Nov. 2020, doi: 10.1016/j.solener.2020.10.036.

[82]   X. Du *et al.*, "Overcoming Interfacial Losses in Solution-Processed Organic Multi-Junction Solar Cells," *Adv. Energy Mater.*, vol. 7, no. 5, p. 1601959, Mar. 2017, doi: 10.1002/aenm.201601959.

[83]   Y. Wang, J. Han, L. Cai, N. Li, Z. Li, and F. Zhu, "Efficient and stable operation of nonfullerene organic solar cells: retaining a high built-in potential," *J. Mater. Chem. A*, vol. 8, no. 40, pp. 21255–21264, 2020, doi: 10.1039/D0TA08018G.

[84]   X. G. Mbuyise, E. A. A. Arbab, K. Kaviyarasu, G. Pellicane, M. Maaza, and G. T. Mola, "Zinc oxide doped single wall carbon nanotubes in hole transport buffer layer," *J. Alloys Compd.*, vol. 706, pp. 344–350, Jun. 2017, doi: 10.1016/j.jallcom.2017.02.249.

[85]   L. Sun *et al.*, "Flexible All-Solution-Processed Organic Solar Cells with High-Performance Nonfullerene Active Layers," *Adv. Mater.*, vol. 32, no. 14, p. 1907840, Apr. 2020, doi: 10.1002/adma.201907840.

[86]   G. Ji *et al.*, "Fully Coated Semitransparent Organic Solar Cells with a Doctor-Blade-Coated Composite Anode Buffer Layer of Phosphomolybdic Acid and PEDOT:PSS and

a Spray-Coated Silver Nanowire Top Electrode," *ACS Appl. Mater. Interfaces*, vol. 10, no. 1, pp. 943–954, Jan. 2018, doi: 10.1021/acsami.7b13346.

[87]  Z. Liu, S. Niu, and N. Wang, "Oleylamine-functionalized graphene oxide as an electron block layer towards high-performance and photostable fullerene-free polymer solar cells," *Nanoscale*, vol. 9, no. 42, pp. 16293–16304, 2017, doi: 10.1039/C7NR05939F.

[88]  S. Maity and T. Thomas, "Hole-Collecting Treated Graphene Layer and PTB7:PC 71 BM-Based Bulk-Heterojunction OPV With Improved Carrier Collection and Photovoltaic Efficiency," *IEEE Trans. Electron Devices*, vol. 65, no. 10, pp. 4548–4554, Oct. 2018, doi: 10.1109/TED.2018.2864537.

[89]  M. Hilal and J. I. Han, "Enhancing the photovoltaic characteristics of organic solar cells by introducing highly conductive graphene as a conductive platform for a PEDOT:PSS anode interfacial layer," *J. Mater. Sci. Mater. Electron.*, vol. 30, no. 6, pp. 6187–6200, Mar. 2019, doi: 10.1007/s10854-019-00921-0.

[90]  T. A. Amollo, G. T. Mola, and V. O. Nyamori, "High-performance organic solar cells utilizing graphene oxide in the active and hole transport layers," *Sol. Energy*, vol. 171, pp. 83–91, Sep. 2018, doi: 10.1016/j.solener.2018.06.068.

[91]  M. Goumri, B. Lucas, B. Ratier, and M. Baitoul, "Inverted Polymer Solar Cells with a Reduced Graphene Oxide/Poly (3,4-Ethylene Dioxythiophene):Poly(4-Styrene Sulfonate) (PEDOT:PSS) Hole Transport Layer," *J. Electron. Mater.*, vol. 48, no. 2, pp. 1097–1105, Feb. 2019, doi: 10.1007/s11664-018-06841-9.

[92]  S. Ozcan, M. C. Erer, S. Vempati, T. Uyar, L. Toppare, and A. Çırpan, "Graphene oxide-doped PEDOT:PSS as hole transport layer in inverted bulk heterojunction solar cell," *J. Mater. Sci. Mater. Electron.*, vol. 31, no. 4, pp. 3576–3584, Feb. 2020, doi: 10.1007/s10854-020-02906-w.

[93]  T. A. Amollo, G. T. Mola, and V. O. Nyamori, "Polymer solar cells with reduced graphene oxide–germanium quantum dots nanocomposite in the hole transport layer," *J. Mater. Sci. Mater. Electron.*, vol. 29, no. 9, pp. 7820–7831, May 2018, doi: 10.1007/s10854-018-8781-1.

[94]  G. R. P., S. R. V., A. Kanwat, and J. Jang, "Enhanced organic photovoltaic properties via structural modifications in PEDOT:PSS due to graphene oxide doping," *Mater. Res.*

*Bull.*, vol. 74, pp. 346–352, Feb. 2016, doi: 10.1016/j.materresbull.2015.10.044.

[95] S. K. Srivastava and J. Pionteck, "Recent Advances in Preparation, Structure, Properties and Applications of Graphite Oxide," *J. Nanosci. Nanotechnol.*, vol. 15, no. 3, pp. 1984–2000, Mar. 2015, doi: 10.1166/jnn.2015.10047.

[96] S. Y. Toh, K. S. Loh, S. K. Kamarudin, and W. R. W. Daud, "Graphene production via electrochemical reduction of graphene oxide: Synthesis and characterisation," *Chem. Eng. J.*, vol. 251, pp. 422–434, 2014, doi: 10.1016/j.cej.2014.04.004.

[97] A. Iwan *et al.*, "Electrochemical and photocurrent characterization of polymer solar cells with improved performance after GO addition to the PEDOT:PSS hole transporting layer," *Sol. Energy*, vol. 146, pp. 230–242, Apr. 2017, doi: 10.1016/j.solener.2017.02.032.

[98] S. Rafique, S. M. Abdullah, M. M. Shahid, M. O. Ansari, and K. Sulaiman, "Significantly improved photovoltaic performance in polymer bulk heterojunction solar cells with graphene oxide /PEDOT:PSS double decked hole transport layer," *Sci. Rep.*, vol. 7, no. 1, p. 39555, Apr. 2017, doi: 10.1038/srep39555.

[99] M. Hilal and J. I. Han, "Significant improvement in the photovoltaic stability of bulk heterojunction organic solar cells by the molecular level interaction of graphene oxide with a PEDOT: PSS composite hole transport layer," *Sol. Energy*, vol. 167, pp. 24–34, Jun. 2018, doi: 10.1016/j.solener.2018.03.083.

[100] B. J. Moon *et al.*, "Multi-functional nitrogen self-doped graphene quantum dots for boosting the photovoltaic performance of BHJ solar cells," *Nano Energy*, vol. 34, pp. 36–46, Apr. 2017, doi: 10.1016/j.nanoen.2017.02.013.

[101] S. Rafique *et al.*, "UV- ozone treated graphene oxide/ PEDOT:PSS bilayer as a novel hole transport layer in highly efficient and stable organic solar cells," *Org. Electron.*, vol. 66, pp. 32–42, Mar. 2019, doi: 10.1016/j.orgel.2018.12.005.

[102] K. Dericiler, H. M. Alishah, S. Bozar, S. Güneş, and F. Kaya, "A novel method for graphene synthesis via electrochemical process and its utilization in organic photovoltaic devices," *Appl. Phys. A*, vol. 126, no. 11, p. 904, Nov. 2020, doi: 10.1007/s00339-020-04091-3.

[103] W. Xing *et al.*, "PEDOT:PSS-Assisted Exfoliation and Functionalization of 2D

Nanosheets for High-Performance Organic Solar Cells," *Adv. Funct. Mater.*, vol. 27, no. 32, p. 1701622, Aug. 2017, doi: 10.1002/adfm.201701622.

[104] D. Koo *et al.*, "Improved charge transport via WSe 2 -mediated hole transporting layer toward efficient organic solar cells," *Semicond. Sci. Technol.*, vol. 33, no. 12, p. 125020, Dec. 2018, doi: 10.1088/1361-6641/aaeab1.

[105] M. S. Ramasamy *et al.*, "Solution-Processed PEDOT:PSS/MoS2 Nanocomposites as Efficient Hole-Transporting Layers for Organic Solar Cells," *Nanomaterials*, vol. 9, no. 9, p. 1328, Sep. 2019, doi: 10.3390/nano9091328.

[106] Y. Dang *et al.*, "Hole Extraction Enhancement for Efficient Polymer Solar Cells with Boronic Acid Functionalized Carbon Nanotubes doped Hole Transport Layers," *ACS Sustain. Chem. Eng.*, vol. 6, no. 4, pp. 5122–5131, Apr. 2018, doi: 10.1021/acssuschemeng.7b04791.

[107] Q. Yang *et al.*, "Boosting Performance of Non-Fullerene Organic Solar Cells by 2D g-C 3 N 4 Doped PEDOT:PSS," *Adv. Funct. Mater.*, vol. 30, no. 15, p. 1910205, Apr. 2020, doi: 10.1002/adfm.201910205.

[108] W. Zhang *et al.*, "Strongly enhanced efficiency of polymer solar cells through unzipped SWNT hybridization in the hole transport layer," *RSC Adv.*, vol. 10, no. 42, pp. 24847–24854, 2020, doi: 10.1039/d0ra03461d.

[109] C. Hou and H. Yu, "Modifying the nanostructures of PEDOT:PSS/Ti 3 C 2 T X composite hole transport layers for highly efficient polymer solar cells," *J. Mater. Chem. C*, vol. 8, no. 12, pp. 4169–4180, 2020, doi: 10.1039/D0TC00075B.

[110] J. W. Jo *et al.*, "Development of Self-Doped Conjugated Polyelectrolytes with Controlled Work Functions and Application to Hole Transport Layer Materials for High-Performance Organic Solar Cells," *Adv. Mater. Interfaces*, vol. 3, no. 12, p. 1500703, Jun. 2016, doi: 10.1002/admi.201500703.

[111] J. W. Jo, J. H. Yun, S. Bae, M. J. Ko, and H. J. Son, "Development of a conjugated donor-acceptor polyelectrolyte with high work function and conductivity for organic solar cells," *Org. Electron.*, vol. 50, pp. 1–6, Nov. 2017, doi: 10.1016/j.orgel.2017.07.006.

[112] Y. Cui, B. Xu, B. Yang, H. Yao, S. Li, and J. Hou, "A Novel pH Neutral Self-Doped

Polymer for Anode Interfacial Layer in Efficient Polymer Solar Cells," *Macromolecules*, vol. 49, no. 21, pp. 8126–8133, Nov. 2016, doi: 10.1021/acs.macromol.6b01595.

[113] M.-H. Choi, E. J. Lee, J. P. Han, and D. K. Moon, "Solution-processed pH-neutral conjugated polyelectrolytes with one-atom variation (O, S, Se) as a novel hole-collecting layer in organic photovoltaics," *Sol. Energy Mater. Sol. Cells*, vol. 155, pp. 243–252, Oct. 2016, doi: 10.1016/j.solmat.2016.06.017.

[114] H. Xu *et al.*, "Highly and homogeneously conductive conjugated polyelectrolyte hole transport layers for efficient organic solar cells," *J. Mater. Chem. A*, vol. 5, no. 28, pp. 14689–14696, 2017, doi: 10.1039/C7TA02590D.

[115] S. Moon, S. Khadtare, M. Wong, S.-H. Han, G. C. Bazan, and H. Choi, "Hole transport layer based on conjugated polyelectrolytes for polymer solar cells," *J. Colloid Interface Sci.*, vol. 518, pp. 21–26, 2018, doi: 10.1016/j.jcis.2018.02.009.

[116] Q. Xie *et al.*, "Self-doped polymer with fluorinated phenylene as hole transport layer for efficient polymer solar cells," *Org. Electron.*, vol. 61, pp. 207–214, Oct. 2018, doi: 10.1016/j.orgel.2018.05.048.

[117] E. J. Lee, M. H. Choi, Y. W. Han, and D. K. Moon, "Effect on Electrode Work Function by Changing Molecular Geometry of Conjugated Polymer Electrolytes and Application for Hole-Transporting Layer of Organic Optoelectronic Devices," *ACS Appl. Mater. Interfaces*, vol. 9, no. 50, pp. 44060–44069, Dec. 2017, doi: 10.1021/acsami.7b11164.

[118] H. Xu *et al.*, "Printable Hole Transport Layer for 1.0 cm 2 Organic Solar Cells," *ACS Appl. Mater. Interfaces*, vol. 12, no. 46, pp. 52028–52037, Nov. 2020, doi: 10.1021/acsami.0c16124.

[119] G.-C. Chiou *et al.*, "Fluorene Conjugated Polymer/Nickel Oxide Nanocomposite Hole Transport Layer Enhances the Efficiency of Organic Photovoltaic Devices," *ACS Appl. Mater. Interfaces*, vol. 9, no. 3, pp. 2232–2239, Jan. 2017, doi: 10.1021/acsami.6b10508.

[120] Y. Guo, H. Lei, L. Xiong, B. Li, and G. Fang, "Organic solar cells based on a Cu 2 O/FBT-TH4 anode buffer layer with enhanced power conversion efficiency and ambient stability," *J. Mater. Chem. C*, vol. 5, no. 32, pp. 8033–8040, 2017, doi:

10.1039/C7TC02566A.

[121] W. J. Jo *et al.*, "Oxidative Chemical Vapor Deposition of Neutral Hole Transporting Polymer for Enhanced Solar Cell Efficiency and Lifetime," *Adv. Mater.*, vol. 28, no. 30, pp. 6399–6404, Aug. 2016, doi: 10.1002/adma.201601221.

[122] H. Awada *et al.*, "Surface engineering of ITO electrode with a functional polymer for PEDOT:PSS-free organic solar cells," *Org. Electron.*, vol. 57, pp. 186–193, Jun. 2018, doi: 10.1016/j.orgel.2018.03.004.

[123] B. Y. Kadem, R. G. Kadhim, and H. Banimuslem, "Efficient P3HT:SWCNTs hybrids as hole transport layer in P3HT:PCBM organic solar cells," *J. Mater. Sci. Mater. Electron.*, vol. 29, no. 11, pp. 9418–9426, Jun. 2018, doi: 10.1007/s10854-018-8974-7.

[124] Z. Babaei, B. Rezaei, M. K. Pisheh, and F. Afshar-Taromi, "In situ synthesis of gold/silver nanoparticles and polyaniline as buffer layer in polymer solar cells," *Mater. Chem. Phys.*, vol. 248, p. 122879, Jul. 2020, doi: 10.1016/j.matchemphys.2020.122879.

[125] L. Deng, D. Li, and S. Agbolaghi, "Networked Conductive Polythiophene/Polyaniline Bottlebrushes with Modified Carbon Nanotubes As Hole Transport Layer in Organic Photovoltaics," *J. Electron. Mater.*, vol. 49, no. 2, pp. 937–948, Feb. 2020, doi: 10.1007/s11664-019-07852-w.

[126] N. Sorkhishams, B. Massoumi, M. Saraei, and S. Agbolaghi, "Electrode buffer layers via networks of polythiophene/polyaniline bottlebrushes and carbon nanotubes in organic solar cells," *J. Mater. Sci. Mater. Electron.*, vol. 30, no. 24, pp. 21117–21125, Dec. 2019, doi: 10.1007/s10854-019-02482-8.

[127] S. Biswas *et al.*, "Decent efficiency improvement of organic photovoltaic cell with low acidic hole transport material by controlling doping concentration," *Appl. Surf. Sci.*, vol. 512, p. 145700, May 2020, doi: 10.1016/j.apsusc.2020.145700.

[128] S. Biswas, Y.-J. You, Y. Lee, J. W. Shim, and H. Kim, "Efficiency improvement of indoor organic solar cell by optimization of the doping level of the hole extraction layer," *Dye. Pigment.*, vol. 183, p. 108719, Dec. 2020, doi: 10.1016/j.dyepig.2020.108719.

[129] S. Biswas, Y.-J. You, J. W. Shim, and H. Kim, "Utilization of poly (4-styrenesulfonic acid) doped polyaniline as a hole transport layer of organic solar cell for indoor applications," *Thin Solid Films*, vol. 700, p. 137921, Apr. 2020, doi:

10.1016/j.tsf.2020.137921.

[130] O. A. Abdulrazzaq, S. E. Bourdo, V. Saini, and A. S. Biris, "Acid-free polyaniline:graphene-oxide hole transport layer in organic solar cells," *J. Mater. Sci. Mater. Electron.*, 2020, doi: 10.1007/s10854-020-04677-w.

[131] J. Dong *et al.*, "A Low-Temperature Solution-Processed CuSCN/Polymer Hole Transporting Layer Enables High Efficiency for Organic Solar Cells," *ACS Appl. Mater. Interfaces*, vol. 12, no. 41, pp. 46373–46380, Oct. 2020, doi: 10.1021/acsami.0c12845.

[132] L. Bormann, F. Selzer, N. Weiß, D. Kneppe, K. Leo, and L. Müller-Meskamp, "Doped hole transport layers processed from solution: Planarization and bridging the voids in noncontinuous silver nanowire electrodes," *Org. Electron.*, vol. 28, pp. 163–171, Jan. 2016, doi: 10.1016/j.orgel.2015.10.007.

[133] J. Cheng *et al.*, "Pre- and post-treatments free nanocomposite based hole transport layer for high performance organic solar cells with considerably enhanced reproducibility," *Nano Energy*, vol. 34, pp. 76–85, Apr. 2017, doi: 10.1016/j.nanoen.2017.02.021.

[134] M. Courté, M. Alaaeddine, V. Barth, L. Tortech, and D. Fichou, "Structural and electronic properties of 2,2′,6,6′-tetraphenyl-dipyranylidene and its use as a hole-collecting interfacial layer in organic solar cells," *Dye. Pigment.*, vol. 141, pp. 487–492, 2017, doi: 10.1016/j.dyepig.2017.03.002.

[135] L. Wang *et al.*, "An organic semiconductor as an anode-buffer for the improvement of small molecular photovoltaic cells," *RSC Adv.*, vol. 7, no. 61, pp. 38204–38209, 2017, doi: 10.1039/C7RA06692A.

[136] J. Li, Y. Zheng, D. Zheng, and J. Yu, "Effect of organic small-molecule hole injection materials on the performance of inverted organic solar cells," *J. Photonics Energy*, vol. 6, no. 3, p. 35502, Aug. 2016, doi: 10.1117/1.JPE.6.035502.

[137] P. Li *et al.*, "Improved charge transport ability of polymer solar cells by using NPB/MoO3 as anode buffer layer," *Sol. Energy*, vol. 170, pp. 212–216, Aug. 2018, doi: 10.1016/j.solener.2018.04.020.

[138] Z. Shi *et al.*, "An alternative hole extraction layer for inverted organic solar cells," *Appl. Phys. A*, vol. 124, no. 10, p. 676, Oct. 2018, doi: 10.1007/s00339-018-2100-9.

[139] S. Wang *et al.*, "A new dibenzo[g.p]chrysene derivative as an efficient anode buffer for

inverted polymer solar cells," *Org. Electron.*, vol. 74, pp. 269–275, Nov. 2019, doi: 10.1016/j.orgel.2019.07.022.

[140] L. Liu *et al.*, "TTA as a potential hole transport layer for application in conventional polymer solar cells," *J. Energy Chem.*, vol. 42, pp. 210–216, Mar. 2020, doi: 10.1016/j.jechem.2019.07.005.